Publication Year	2015
Acceptance in OA	2024-01-25T14:41:34Z
Title	Lick-index entanglement and biased diagnostic of stellar populations in galaxies
Authors	BUZZONI, Alberto
Publisher's version (DOI)	10.1093/mnras/stv242
Handle	http://hdl.handle.net/20.500.12386/34629
Journal	MONTHLY NOTICES OF THE ROYAL ASTRONOMICAL SOCIETY
Volume	449

Monthly Notices
of the
ROYAL ASTRONOMICAL SOCIETY

MNRAS **449,** 296–315 (2015) doi:10.1093/mnras/stv242

Lick-index entanglement and biased diagnostic of stellar populations in galaxies*

Alberto Buzzoni†

INAF - Osservatorio Astronomico di Bologna, Via Ranzani 1, I-40127 Bologna, Italy

Accepted 2015 February 4. Received 2015 January 8; in original form 2014 September 8

ABSTRACT

The inherent statistical and operational properties of the Lick-index spectrophotometric system are investigated to facilitate a more appropriate use for astrophysical studies. Non-Gaussian effects in the index standardization procedure suggest that a minimum S/N ratio has to be met by spectral data, such as $S/N \gtrsim 5$ px^{-1} for a spectral resolution $R \sim 2000$. In addition, index (re-)definition in terms of narrow-band colour should be preferred over the classical pseudo-equivalent width scheme. The overlapping wavelength range among different indices is also an issue, as it may lead the later ones to correlate beyond any strictly physical relationship. The nested configuration of the Fe5335 and Fe5270 indices, and the so-called Mg complex (including Mg$_1$, Mg$_2$ and Mg*b*), is analysed, in this context, by assessing the implied bias when joining entangled features into global diagnostic meta-indices, like the perused [MgFe] metallicity tracer. The perturbing effect of [O III]$_{5007}$ and [N I]$_{5199}$ forbidden gas emission on Fe5015 and Mg*b* absorption features is considered, and an updated correction scheme is proposed when using [O III]$_{5007}$ as a proxy to appraise Hβ residual emission. When applied to the present-day elliptical galaxy population, the revised Hβ scale leads, on average, to 20–30 per cent younger age estimates. Finally, the misleading role of the christening element in Lick-based chemical analyses is illustrated for the striking case of Fe4531. In fact, while iron is nominally the main contributor to the observed feature in high-resolution spectra, we have shown that the maximum responsiveness of the Fe4531 index is actually to titanium abundance.

Key words: methods: observational – techniques: spectroscopic – galaxies: elliptical and lenticular, cD – galaxies: fundamental parameters – galaxies: photometry.

1 INTRODUCTION

Since the beginning, the Lick-index system was intentionally conceived as a tool to characterize elliptical galaxies and other old stellar systems (Faber, Burstein & Dressler 1977; Faber et al. 1985; Davies et al. 1987; Gorgas, Efstathiou & Aragon Salamanca 1990). Only a few relevant absorption lines were originally taken into account, at the sides of the strong magnesium feature around 5175 Å, which blends the molecular hydride MgH and the atomic doublet Mg*b* (Mould 1978). Together with the 4000 Å break, the Mg ‘valley’ has since long been recognized as the most outstanding pattern in the optical spectrum of galaxies (Öhman 1934; Wood 1963; Spinrad & Wood 1965).

The immediate interest for galaxy investigation directly drove a parallel effort to extend the index data base also to cool stars (e.g., Burstein et al. 1984) because of the evident link with the study of old galaxies through population synthesis applications. At the same time, this also led to a more definite treatment of the whole index system, greatly extended by new additions from the Lick Image Dissector Scanner (IDS) data archive including all the relevant absorption features in the optical wavelength range between the 4000 Å break and the Balmer Hα line (Gorgas et al. 1993; Worthey et al. 1994). The original emphasis on old stellar populations was extended to hot and warm stars (Worthey & Ottaviani 1997) to account for ongoing star formation scenarios, as in late-type galaxies (e.g., Mollá, Hardy & Beauchamp 1999; Walcher et al. 2006; Pérez, Sánchez-Blázquez & Zurita 2009).

In more recent years, other spectroscopic methods have complemented the original Lick approach, aiming to tackle galaxy properties at a finer or coarser detail. High-resolution spectroscopy (say at the typical resolving power, $R \gtrsim 2000$ or so, of current extragalactic surveys) certainly added valuable clues. On the opposite

---

*Also based on observations made at the Observatorio Astronómico G. Haro of INAOE, Cananea (Mexico)

† E-mail: alberto.buzzoni@oabo.inaf.it

Published by Oxford University Press on behalf of the Royal Astronomical Society

side, a panchromatic analysis relying on low-resolution fitting of galaxy spectral energy distributions (SEDs) (often assembled by straight flux conversion of integrated broad-band magnitudes) also became an increasingly popular way to deal with the massive wealth of galaxy data, characterizing red shift distribution and other outstanding evolutionary features on a statistical basis (see Walcher et al. 2011; Conroy 2013, for excellent reviews of these subjects).

For several reasons, however, none of these techniques is free from limitations. High-resolution spectroscopy may be constrained by the intervening role of galaxy dynamics; at a typical velocity dispersion of $\sigma_{\rm v} \simeq 300\,{\rm km\,s^{-1}}$, the induced line broadening limits the effective resolving power to $R \lesssim 1000$. On the other hand, global fitting of galaxy SED carries all the inherent uncertainty in absolute flux calibration of the observations, especially when matching data from different observing sources and over distant wavelength ranges. In addition, to quote Walcher et al. (2011), we have to remember that as 'the uncertainties are dominated by the uncertainties in the SED modelling itself, thus one has to be very cautious about the interpretations when selecting samples where a specific type of model is preferred.'

For all these reasons, narrow-band spectrophotometry still remains, in most cases, the chosen (and often the only viable) tool to assess in finer detail the evolutionary status of galaxies and other unresolved stellar aggregates both in local and high-red-shift environments (see Bernardi et al. 2006; Carson & Nichol 2010; Dobos et al. 2012, for recent contributions). Such a broad range of applications, however, urges a more careful in-depth analysis of the inherent properties of the Lick system to enable its appropriate use in the investigation of single stars and integrated stellar systems. This motivated the present work.

When dealing with Lick indices, two intervening difficulties may in principle affect our conclusions. A first, and often underrated issue (discussed here in Section 2) is index *standardization*, which is the process of making index measurements from different sources or observing circumstances compare consistently with each other. Quite importantly, this process should not be confused with the *calibration* procedure, as the first requires *ab initio* that index definition could lead at any time to a fair statistical realization of a normal statistical variable according to the central limit theorem (see, e.g., Sachs 1984, for a rigorous theoretical treatment of the problem). While satisfactory attention is paid in the relevant literature to the suitable calibration of observing data (Worthey et al. 1994; Trager et al. 1998; Cardiel et al. 1998), this cannot ensure, by itself, that a standard treatment of the derived index estimates is always achieved.

The next feature we have to consider is that indices may not be completely *independent* of each other, and we will show in Section 3 that some degree of redundancy occurs in many cases. For instance, sometimes two indices may share the same pseudo-continuum window, or two feature windows are partly or fully superposed, etc. Even more sneakily, some redundancy may also appear when, under certain conditions, the chemical element that constrains the main feature also affects the surrounding pseudo-continuum, thus masking the sensitivity of the index to its abundance or making it vanish. When the temperature or another fundamental parameter of a star changes, a hidden chemical element may abruptly appear at some point with its lines, and superpose on the other absorption features, thus affecting the corresponding indices. This is, for instance, the classical case of the onset of TiO molecular bands in cool stars, which perturb, among others, the Mg_2 and Fe5270 indices (Buzzoni, Gariboldi & Mantegazza 1992; Tantalo & Chiosi 2004; Buzzoni, Bertone & Chavez 2009a).

A further range of problems relates to the physical environment of stellar populations. Most importantly, a natural effect of fresh star formation on the integrated spectrum of galaxies is line emission driven by the residual interstellar gas. Along the Lick-index range, this results in enhanced hydrogen Balmer lines and, depending on the overall thermodynamic conditions, also in [O III] forbidden emission at 4363, 4959 and 5007 Å (see Kennicutt 1992, for excellent explanatory examples). On the other hand, oxygen and Hβ emission is triggered even at the vanishing star formation rates observed in most elliptical galaxies (Caldwell 1984; Phillips et al. 1986; Bettoni & Buson 1987; Volkov 1990; Sarzi et al. 2010; Crocker et al. 2011) due, at the very least, to the contribution of the planetary nebulae (see Kehrig et al. 2012, for an example), and this could easily bias our conclusions if we use Hβ (absorption) strength to constrain galaxy age.

In this paper we will carry on our analysis from two independent points of view, starting from the expected behaviour according to index properties and checking theoretical predictions with a tuned set of spectroscopic observations for a sample of 20 elliptical galaxies. Our relevant conclusions, and a reasoned summary of the manifold variables at work, are proposed in Section 4 of the paper.

2 INDEX TECHNICALITIES

Up to the 1970s, low-resolution sampling of galaxy and stellar energy distribution was mainly pursued by narrow-band photometry. Popular multicolour systems included, for instance, those of Strömgren (1956), the DDO system of McClure & van den Bergh (1968), the multicolour set of Spinrad & Taylor (1969) or the 10-colour system of Faber (1973). In this framework, the Lick system stands out for its innovative approach to the problem, tackled now from a purely spectroscopic point of view.

Indeed, such a new spectroscopic mood is inherent in the Lick-index definition. The procedure applies to low-resolution spectra ($R \sim 500$) and aims to derive the strength of a number of absorption features through a measure of their pseudo-equivalent width. Indices are therefore measured in Å, maintaining the magnitude scale only for a few molecular bands (Worthey et al. 1994). The original set of 21 indices was defined by Worthey et al. (1994) and slightly adapted to fit extragalactic targets better by Trager et al. (1998). A complement to include the full Balmer line series in the optical wavelength range led Worthey & Ottaviani (1997) to add four new indices, which match the Hγ and Hδ lines with narrow and wide windows. With these additions, the full Lick system consists of 25 indices. Otherwise, it is worth including in our analysis also an ad hoc addition to the standard set due to González (1993), to account for [O III] emission in the spectrum of star-forming galaxies. Note that this is the only index aimed at measuring an emission feature (see Fig. 1).

According to original precepts in Worthey et al. (1994), the key quantity of any Lick index is the ratio

$$\mathcal{R} = \overline{\left(\frac{f}{f_c}\right)} = \frac{1}{w}\int_w \left(\frac{f}{f_c}\right)_\lambda \,\mathrm{d}\lambda. \quad (1)$$

$\mathcal{R}$ is therefore an average, along the w-wide feature window, of the apparent flux density, $f(\lambda)$, normalized to the (pseudo-)continuum level, $f_c(\lambda)$, linearly interpolated at the same wavelength. Two adjacent bands, on both sides of the feature, provide the baseline for the interpolated process. With these prescriptions, the index then directly follows either as

$$I(\text{Å}) = w\,(1 - \mathcal{R}) \quad (2)$$

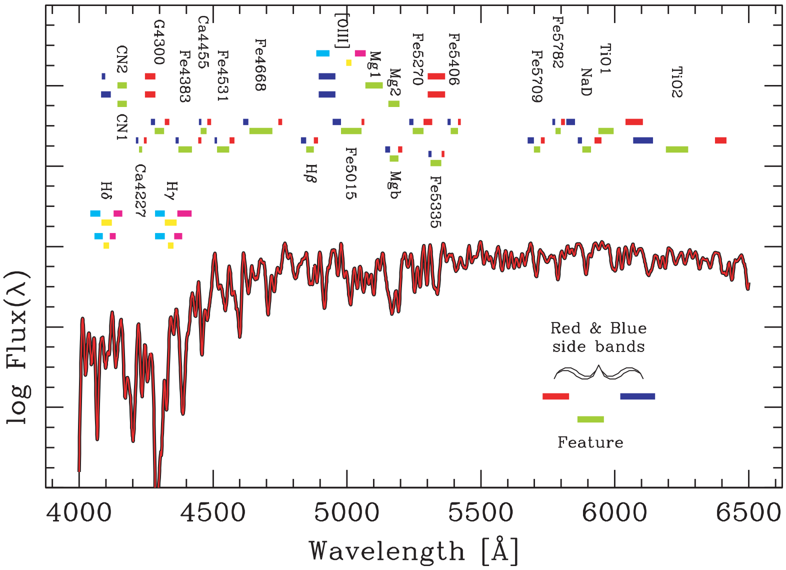

Figure 1. A global view of the Lick-index wavelength distribution. The original set of 21 indices (Worthey et al. 1994) has been complemented by four new Balmer indices of Worthey & Ottaviani (1997) (namely, Hδ and Hγ, in their wide and narrow versions) and the [O III] index of González (1993), as labelled in the plot. The index map is superposed on a synthetic stellar spectrum with [$T_{\rm eff}$, log g, Z] = [4750 K, 2.00, $Z_\odot$] from the BLUERED theoretical library (Bertone et al. 2004, 2008), degraded to match the Lick spectral resolution of 8.5 Å full width at half-maximum (FWHM).

or

$$I(\mathrm{mag}) = -2.5 \log \mathcal{R} \qquad (3)$$

depending whether we want to express it in Å, as a pseudo-equivalent width, or in magnitude scale. Clearly, both definitions are fully equivalent and easily reversible as

$$I(\text{Å}) = w \left[1 - 10^{-0.4 I(\mathrm{mag})}\right] \qquad (4)$$

or

$$I(\mathrm{mag}) = -2.5 \log \left[1 - \frac{I(\text{Å})}{w}\right], \qquad (5)$$

and the use of Å or magnitudes is just a matter of ‘flavour’, as we have mentioned above (see, for instance, Brodie & Huchra 1990, Colless et al. 1999, or Sánchez-Blázquez et al. 2006a for alternative non-standard notations). As a rule, both equations (2) and (3) are positive for absorption features and negative for emission ones.

2.1 Standardization constraints

In spite of its established popularity and extensive use in a broad range of stellar and extragalactic studies, a well-recognized drawback of the Lick system is its ambiguous standardization procedure. A meticulous analysis of this has been attempted by Trager et al. (1998) to account for the macroscopic limits of the IDS data base due to the somewhat fickle technical performance of the instrument. Some inconstancy in the spectrum wavelength scale is, for instance, a recognized issue, and even the spectral resolution (about 8.5 Å FWHM, see Worthey & Ottaviani 1997) cannot be firmly established due to the slightly unpredictable behaviour of the instrument output with time (Worthey et al. 1994). In addition, and quite importantly, notice that the whole IDS data set is in fact *not* flux-calibrated (Worthey et al. 1994), thus taking over the instrument (slightly variable) response curve. For all these reasons, any comparison between external data sources in the literature must necessarily rely, *as a minimum*, on the observation of a common grid of standard stars (e.g., Buzzoni et al. 1992; Gorgas et al. 1993; Worthey et al. 1994; Buzzoni, Mantegazza & Gariboldi 1994; Buzzoni et al. 2001, among others).

A few attempts have been made, in the recent literature, to refine the index estimates from the operational point of view to secure on a more solid basis the observed output. The work of Rogers et al. (2010) is certainly the most relevant one, in this regard, as it especially focuses on the problem of a fair treatment of the pseudo-continuum level (through the so-called boosted median continuum method) to derive a more confident feature strength, also overcoming those recognized cases of unphysical output (for example, with nominal emission indices tracing absorption features, etc.).

As a matter of fact, any more or less elaborated empirical matching procedure, however, cannot overcome a more subtle but inherent difficulty in the standardization process of the Lick system. In fact, computing $\mathcal{R}$ according to equation (1) is a direct heritage of high-resolution spectroscopy, where the measure is always carried out on preliminarily continuum-rectified spectra. However, this is clearly *not* the case for the (unfluxed) Lick spectra, where possibly steep continuum gradients are, in principle, an issue. According to statistics theory, the consequence is that ratio $\mathcal{R}$ may display strongly non-Gaussian properties (see Marsiglia 1964, and especially fig. 1 therein for an eloquent example), making the analysis of its distribution a hard (and in some cases hopeless) task. In other words, this implies that, in general, any effort to reproduce the system may not obey the central limit theorem so that its convergence is not assured a priori (Marsiglia 1965).

In this framework, it is therefore of central interest to explore the real constraints that make $\mathcal{R}$ behave normally. For this, let us briefly consider the more general problem of the stochastic behaviour of a statistical variable r being the ratio of two normal variables x and y, namely $r = y/x$. It has been firmly demonstrated (Geary 1930; Hinkley 1969; Hayya, Armstrong & Gressis 1975) that r tends to behave like y if the range of variation of x (that is $\mathrm{d}x/\overline{x}$), approaches zero and the x variable is ‘unlikely to assume negative values’ (Geary 1930). If this is the case, then x tends to behave as a (positive) constant, and xr would resemble the y distribution (Hayya et al. 1975). Under these assumptions, the $r' = \overline{y}/\overline{x}$ ratio will display a normal distribution and its average $\overline{r'}$ tends to be an unbiased proxy of $\overline{r}$. In our terms, therefore, the crucial constraints that ensure both index Gaussianity and its fair reproducibility directly deal with two issues: on one hand we need a small range of variation for $\mathrm{d}f_c/\overline{f_c}$; on the other hand, we need to assess the condition for which $\overline{r'} \to \overline{r}$.

To proceed with our analysis further, let us preliminarily assume the relative variation of f_c *to be* small, indeed, so that we can set up a linear expansion for f_c around λ_o, the central wavelength within the feature window of width w:

$$\frac{1}{f_c} = \left[\frac{1}{\overline{f_c}} - \frac{1}{\overline{f_c}^2}\frac{\partial f_c}{\partial \lambda}(\lambda - \lambda_o)\right] = \frac{1}{\overline{f_c}}\left[1 - \frac{\alpha(\lambda - \lambda_o)}{\overline{f_c}}\right]. \tag{6}$$

In the above, $\alpha = \partial f_c/\partial\lambda$ and, by definition, $(\alpha w) = \mathrm{d}f_c$ is the maximum excursion of $f_c(\lambda)$ within the feature window.

By implementing equation (6) into equation (1) we have

$$\mathcal{R} = \frac{1}{\overline{f_c}}\left[\frac{\int_w f(\lambda)\,\mathrm{d}\lambda}{w} - \frac{\alpha}{w\overline{f_c}}\int_w f(\lambda)(\lambda - \lambda_o)\,\mathrm{d}\lambda\right]. \tag{7}$$

If we now multiply out and divide the last term of the equation by $w\int f(\lambda)\,\mathrm{d}\lambda$, with a little arithmetic we can rearrange the equation and write:

$$\mathcal{R} = \mathcal{R}'\left[1 - \frac{\alpha w}{\overline{f_c}}\frac{\langle\delta\lambda\rangle}{w}\right] = \mathcal{R}'\left[1 - \frac{\langle\delta\lambda\rangle}{w}\left(\frac{\mathrm{d}f_c}{\overline{f_c}}\right)^{\max}\right] \tag{8}$$

being

$$\mathcal{R}' = \left(\frac{\overline{f}}{\overline{f_c}}\right), \tag{9}$$

and $\langle\delta\lambda\rangle/w$ is the relative displacement, within the feature window, of the line centroid with respect to λ_o, in consequence of symmetry departure due to the spectral slope. According to equation (8), therefore, $\mathcal{R}'$ tends to become a fair proxy of $\mathcal{R}$ if

$$\left|1 - \frac{\mathcal{R}}{\mathcal{R}'}\right| \lesssim \left(\frac{\langle\delta\lambda\rangle}{w}\right)\left(\frac{\mathrm{d}f_c}{\overline{f_c}}\right)^{\max}. \tag{10}$$

The maximum relative excursion $(\mathrm{d}f_c/\overline{f_c})^{\max}$ is, evidently, the key figure in this process as it directly constrains both right-hand factors in equation (10). It may be wise to assess the allowed range of this parameter in terms of the stochastic fluctuation range of f_c within the same window, the latter being directly related to the signal-to-noise ratio (S/N) of our data, so that we can set

$$\left(\frac{\mathrm{d}f_c}{\overline{f_c}}\right)^{\max} \lesssim k\left[\frac{\sigma(f_c)}{\overline{f_c}}\right] = \frac{k}{S/N}, \tag{11}$$

with k a tuning factor. We will show, in the next section, that a minimum signal-to-noise ratio of $S/N \sim 20$ is required for $\mathcal{R}'$ to behave normally (Hayya et al. 1975). With this figure, if we tentatively choose to accept a pseudo-continuum excursion within a $\pm 3\sigma$ range of the random noise, then $k \lesssim 6$ and $(\mathrm{d}f_c/\overline{f_c})^{\max} \lesssim 0.3$, so that one could actually verify numerically that

$$\left|1 - \frac{\mathcal{R}}{\mathcal{R}'}\right| \lesssim 0.01. \tag{12}$$

With the previous assumptions, this means that, within a 1 per cent accuracy, the ratio $\mathcal{R}'$ eventually becomes an unbiased estimator of $\mathcal{R}$, thus ensuring that $\mathcal{R}$ behaves normally, too. Our first conclusion is therefore that the prescriptions of Geary (1930) require the pseudo-continuum not to exceed a ±30 per cent relative variation within the feature window for any Lick index to obey the central limit theorem, and display a Gaussian distribution.

2.2 Random-error estimate

A range of more or less entangled attempts have been proposed across the literature to derive a general and self-consistent estimate of the statistical uncertainty related to narrow-band indices (Rich 1988; Brodie & Huchra 1990; Carollo, Danziger & Buson 1993; González 1993; Cardiel et al. 1998; Trager et al. 1998). Yet, this effort does not seem to have led to any firm and straightforward pathway to assess the index random-error estimate. Quite different formal approaches can be found among authors depending on whether the intervening noise sources (including photon statistics, flat-fielding procedure, sky subtraction, etc.) are considered individually or at a somewhat aggregated level in the analysis. In addition, as we discussed in the previous section, with the Lick system one has to deal with the duality of the index definition, sometimes seen in terms of pseudo-colours and sometimes in terms of pseudo-equivalent widths.

In its general form, by simple differentiation of equations (2) and (3), the expected internal uncertainty of a Lick index expressed in magnitude is

$$\sigma(I)_{\mathrm{mag}} = 1.08\left[\frac{\sigma(\mathcal{R})}{\mathcal{R}}\right]. \tag{13}$$

In contrast, if we chose to express the index in pseudo-equivalent width, then

$$\sigma(I)_{\mathrm{Å}} = \left[\frac{\sigma(\mathcal{R})}{\mathcal{R}}\right](w - I_{\mathrm{Å}}). \tag{14}$$

In both cases, the crucial quantity that we have to assess is the $\sigma(\mathcal{R})/\mathcal{R}$ ratio. A useful contribution to settle the problem has come from Vollmann & Eversberg (2006), who deal with the error estimate in equivalent-width measurements from high-resolution spectroscopy. In many respects, their results directly apply to our framework providing the caveats of the previous section are properly accounted for in our analysis and we observe at ‘sufficient S/N within the continuum’ (Vollmann & Eversberg 2006). If the $\mathcal{R}'$ ratio is an effective proxy of $\mathcal{R}$, then the variance of $\mathcal{R}$ directly derives from error propagation as

$$\sigma^2(\mathcal{R}) = \left[\frac{\partial\mathcal{R}}{\partial f}\sigma(f)\right]^2 + \left[\frac{\partial\mathcal{R}}{\partial f_c}\sigma(f_c)\right]^2, \tag{15}$$

which implies

$$\sigma^2(\mathcal{R}) = \left(\frac{1}{f_c^2}\sigma_f^2\right) + \left(\frac{f^2}{f_c^4}\sigma_{fc}^2\right) = \frac{f^2}{f_c^2}\,\frac{\sigma_f^2}{f^2} + \frac{f^2}{f_c^2}\,\frac{\sigma_{fc}^2}{f_c^2}. \tag{16}$$

If a similar S/N ratio for the relevant range of our spectrum can be assumed, so that $(\sigma(f)/f) \sim (\sigma(fc)/f_c)$, a final compact form can be achieved for the previous equations such as:

$$\frac{\sigma(\mathcal{R})}{\mathcal{R}} \simeq \frac{\sigma(\mathcal{R})}{\mathcal{R}'} = \frac{\sqrt{2}}{(S/N)_{\mathrm{idx}}}. \tag{17}$$

Quite importantly, note that the value of S/N in equation (17) refers to the *integrated* figure along the feature and continuum windows. Providing we observe a spectrum with an original $(S/N)_{\mathrm{obs}}$ ratio *per pixel* and a dispersion θ Å px^{-1}, the resulting $(S/N)_{\mathrm{idx}}$ by sampling the flux along a window w Å wide is, of course,

$$(S/N)_{\mathrm{idx}} = (S/N)_{\mathrm{obs}}\sqrt{\frac{w}{\theta}}. \tag{18}$$

Table 1. Harmonic average[a] ($\mathcal{W}$), feature (w) and continuum (W) window width for the extended set of Lick indices.

Index	$\mathcal{W}$ [Å]	w [Å]	W [Å]	Index	$\mathcal{W}$ [Å]	w [Å]	W [Å]
$\mathrm{H}\delta_W$	50.1	38.8	70.6	[O III]	32.7	20.0	90.0
$\mathrm{H}\delta_N$	30.5	21.3	53.8	Fe_{5015}	54.6	76.3	42.5
CN_1	48.2	35.0	77.5	Mg_1	86.1	65.0	127.5
CN_2	42.0	35.0	52.5	Mg_2	63.8	42.5	127.5
Ca_{4227}	15.0	12.5	18.8	Mg_b	33.1	32.5	33.7
G_{4300}	33.7	35.0	32.5	Fe_{5270}	43.4	40.0	47.5
$\mathrm{H}\gamma_W$	58.6	43.8	88.8	Fe_{5335}	27.8	40.0	21.2
$\mathrm{H}\gamma_N$	31.9	21.0	66.3	Fe_{5406}	24.0	27.5	21.3
Fe_{4383}	32.5	51.3	23.8	Fe_{5709}	29.1	23.8	37.5
Ca_{4455}	23.1	22.5	23.7	Fe_{5782}	21.7	20.0	23.7
Fe_{4531}	35.1	45.0	28.8	NaD	36.3	32.5	41.0
Fe_{4668}	47.3	86.3	32.5	TiO_1	72.3	57.5	97.5
$\mathrm{H}\beta$	31.6	28.8	35.0	TiO_2	97.0	82.5	117.5

Note. [a] According to equation (21).

In their work, Hayya et al. (1975) set the limit of the general validity of this formal approach through a detailed Monte Carlo analysis. Converting their results to our specific framework (see, in particular, their fig. 1), we conclude that equation (17) is a robust estimator of the relative standard deviation of $\mathcal{R}$ providing we work with $(S/N)_{\rm idx} > 20$.

On the basis of our discussion, we can eventually rearrange equations (13) and (14) into their final form, respectively:

$$\sigma(I)_{\rm mag} = \sqrt{\frac{2\vartheta}{\mathcal{W}}}\ \frac{1.09}{(S/N)_{\rm obs}}, \tag{19}$$

and

$$\sigma(I)_{\rm Å} = \sqrt{\frac{2\vartheta}{\mathcal{W}}}\ \frac{w}{(S/N)_{\rm obs}}\left(1-\frac{I_{\rm Å}}{w}\right). \tag{20}$$

For shallow lines (that is those with $[I(\text{Å})/w] \ll 1$), we can simply neglect the last factor in the previous equation, thus leading to an even more compact (though slightly overestimated) form for the standard deviation.

In both equations (19) and (20), $\mathcal{W}$ is the harmonic average of the feature (w) and continuum (W) window widths:

$$\frac{2}{\mathcal{W}} = \left(\frac{1}{w}+\frac{1}{W}\right). \tag{21}$$

For convenience, the values of $\mathcal{W}$, together with the feature and the full (i.e., red+blue) continuum windows for the extended set of Lick indices, are summarized in Table 1.

Taking equations (19) and (20) as a reference, in Fig. 2 we compare the observed standard deviation of primary Lick stellar calibrators, according to Worthey et al. (1994, see, in particular, their table 1) and Worthey & Ottaviani (1997) with our expected error distribution for a spectrum of $(S/N)_{\rm obs} = 30$.

Although no firm appraisal can be done of original IDS data in terms of the S/N ratio, a problem extensively discussed by Worthey et al. (1994), nonetheless it is reasonable to believe that the S/N assumed in the present derivation is similar to the floor imposed on the IDS spectra by small-scale flat-fielding problems. In this framework one could recognize our statistical analysis as an instructive exercise to put in a more standard context the inherent uncertainty of Worthey et al.'s reference data set, at least for indices redder than ∼4350 Å.

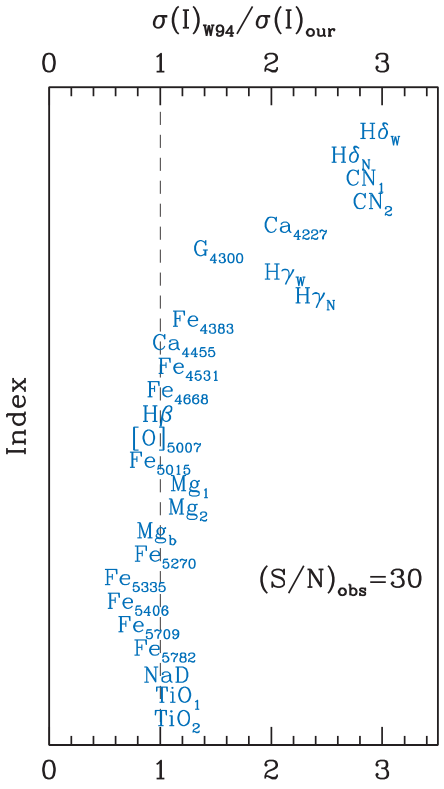

Figure 2. Expected index standard deviation $\sigma(I)_{\rm our}$, according to equation (20), for an assumed spectral $S/N \sim 30$ compared with the empirical estimate from the Lick primary calibrators, as table 1 of Worthey et al. (1994) and Worthey & Ottaviani (1997). The uncertainty for $[\mathrm{O\,III}]_{5007}$ has been estimated from the González (1993) data, from their table 4.1, by scaling down the figures to $S/N = 30$. Notice that Lick IDS spectra lack any stable intensity response, a feature that prevents any firm assessment of the S/N ratio of the original data (Faber & Jackson 1976; Worthey et al. 1994). A remarkably good agreement is found, however, with our theoretical predictions, for the 'red' indices (about $\lambda \gtrsim 4350$ Å). A notable worsening in the Lick calibration accuracy is evident at shorter wavelengths, likely due to poorer detector performance and statistical drawbacks inherent in the index definition, as discussed in the text.

Note, however, a dramatic worsening of the IDS performance in the blue, where index accuracy quickly degrades. This trend can now easily be understood on the basis of our previous statistical arguments. At shorter wavelengths, the combined effects of a worse IDS response and an intrinsic drop of SED for stars of intermediate and late spectral type all conspire to exacerbate any spectral slope, thus departing from the standard Gaussian scenario (following equation 10), and adding further extra volatility to the Lick-index calculation.

3 INDEX ENTANGLEMENT AND REDUNDANCY

A closer look at the data of Fig. 1 shows that about 25 per cent of the covered wavelength range actually contributes to the definition of two or more indices leading, on average, to a 1.5 oversampling fraction. Such a redundancy evidently calls for a more detailed analysis of the possible bias effects that in some cases make indices interdependent in their stochastic fluctuation, that is *beyond any strictly physical relationship.*

There is certainly some intervening emission, which superposes on absorption features (Hβ is a typical example of this). Also partly or fully overlapping pseudo-continuum windows, in common with different indices, may induce some degree of correlation in the corresponding output (e.g., the blue sidebands of Ca4455 and Fe5335 are fully within the Fe4383 and Fe5270 red sidebands, respectively). This may also happen to feature windows, as shown for instance by Mg*b*, which is fully within the Mg$_2$ central band. Finally, a further possibility is that the entire feature contributes to the pseudo-continuum window of another index: Fe5335 is an example, being fully nested in the red sideband of Mg$_2$ and Mg$_1$.

In this section we want, therefore, to assess some illustrative cases giving, when possible, a guideline for a more general application of our results. The theoretical predictions from the reference discussion of Section 2 will be accompanied by an empirical check, which could give a clean assessment of the different situations sketched above.

3.1 Radial spectroscopy of elliptical galaxies as a robust empirical check

For our aims, it is convenient to rely on a set of spectroscopic data for a sample of 20 early-type (mainly elliptical) galaxies observed with the 2.12-m telescope of the G. Haro Observatory of Cananea (Mexico) in a series of runs in 1996 and 1997. These observations are part of a more general exhaustive study on spectroscopic gradients across the surface of galaxies and the physical implications for galaxy evolution (Carrasco et al. 1995; Buzzoni et al. 2009b, 2015). It is clearly beyond the scope of this work to dig further into the original scientific issue and the detailed data reduction analysis (see the cited references for a full review). We just want to recap here the basic information to characterize the sample in view of its possible relevance as an independent tool to probe our theoretical output.

The spectra were collected with a long-slit Böller & Chivens Cassegrain spectrograph equipped with a 300 gr mm^{-1} grating, which provided a dispersion of 67 Å mm^{-1} along a 4200–6000 Å wavelength interval. The spectral resolution was set to 5 Å (FWHM) throughout ($R = \lambda/\Delta\lambda \sim 1000$). Galaxy targets were typically exposed for 1 hr (3 × 1200 arcsec frames) centred along the galaxy's major axis. The resulting spectra were wavelength- and flux-calibrated according to standard procedures, and then rebinned in the spatial domain, so as to sample the galaxy radius at 3–5 values of distance symmetrically placed with respect to the centre, roughly up to one effective radius (see Buzzoni et al. 2009b, for an example). The rebinning procedure allowed us to greatly improve the S/N ratio, especially in the outermost regions, where there $S/N \gtrsim 25$ px^{-1}, a figure that quickly improved to $S/N \gtrsim 80$ px^{-1} towards the centre.

The relevant information of the galaxy sample is summarized in Table 2. From the RC3 catalogue (de Vaucouleurs et al. 1991), we report morphological classification, absolute *B*-band magnitude (M_B) and apparent $(B - V)$ colour within one effective radius (r_e). In addition, in the last two columns we added, the radial fraction sampled with our spectra (r/r_e) (see Buzzoni et al. 2009b, for further details), and a flag for galaxies with reported emission. In this regard, one asterisk marks a confirmed $[\mathrm{O\,II}]_{3727}$ emission, as in the Bettoni & Buson (1987) catalogue, while a double asterisk marks targets with evident $[\mathrm{O\,III}]_{5007}$ and/or Hβ central emission in our spectra.

Table 2. The galaxy data base.

NGC	Type	M_B	$(B - V)$	$r_{\max}/r_e$	Emission?
1587	E1p	−21.19	1.04	0.2	* *
1588	Ep	−19.91	1.00	0.5	
2685	S0-a	−19.09	0.94	0.8	*
2764	S0	−19.55	0.71	1.2	* *
3245	S0	−20.09	0.89	1.0	
3489	S0-a	−19.23	0.85	0.8	* *
3607	E-S0	−20.00	0.93	0.4	*
4111	S0-a	−19.16	0.88	3.0	*
4125	E6p	−21.27	0.94	0.4	*
4278	E1	−19.35	0.96	1.0	* *
4374	E1	−21.05	1.00	0.6	*
4382	S0-a	−20.50	0.89	0.3	
4472	E2	−21.71	0.98	0.8	
4649	E2	−21.47	1.00	0.5	
4742	E4	−19.35	0.79	1.3	*
5576	E3	−20.14	0.90	0.4	
5812	E0	−20.44	1.04	0.4	
5866	S0-a	−20.00	0.93	0.7	* *
5982	E3	−21.38	0.94	0.7	*
6166	E2p	−22.96	1.03	0.4	*

For the galaxies of Table 2, Buzzoni et al. (2009b, 2015) derived the complete set of 17 standard Lick indices (including the $[\mathrm{O\,III}]_{5007}$ feature), from G4300 to Fe5709. These data provide us with a useful reference to perform, for each index, a series of *statistically equivalent realizations*. This can be carried out following the supposed central symmetry of the galaxy spectral properties. Even for spectroscopic radial gradients, in fact, a similar stellar population has to be hosted at the same distance on opposite sides of the galaxy, leading to a nominally identical set of absorption indices. Clearly, any systematic deviation from this pure folding effect may be worth attention in our analysis.

Note that, as we deal with index *differences*, our method is quite insensitive to standardization problems (zero-point treatment, calibration drift, etc.), although we obviously magnify the internal random errors of our analysis by a factor of $\sqrt{2}$. About 80 pairs of index differences have been computed across the full galaxy sample, for a total of roughly 1400 measures for the full set of 17 indices.

As an explanatory example to illustrate our approach, we show in Fig. 3 the Δ–Δ index distribution for two Fe I indices, namely Fe5270 versus Fe4383. Each point in the plot is from the following procedure. For two slices at the same radial distance (and on opposite sides) of a given galaxy, we computed δx as the left–right difference of the Fe4383 index measurements. The same is done for Fe5270, deriving δy. We then set $\Delta x = |\delta x|$ and obtain the sign of δx as $\mathrm{sign}_x = \delta(x)/\Delta(x)$, so that $\Delta y = \mathrm{sign}_x \delta y$. Though, from a physical point of view, both indices should correlate with iron abundance, no mutual influence can exist for their relative variation. As a consequence, their left–right differences must be statistically independent over the entire galaxy sample. This is actually confirmed by the least-squares fit to the data in the figure (68 points in total), which provides $\alpha = 0.03 \pm 0.05$.[1]

---

[1] As a general rule, throughout in our Δ–Δ fits, we applied to *both x* and *y* variables an rms clipping procedure at a 3σ level to reject the catastrophic outliers (residual spikes from cosmic rays in the spectra, cold/warm pixels affecting the index strength, lack of index estimate on either left or right side, etc.).

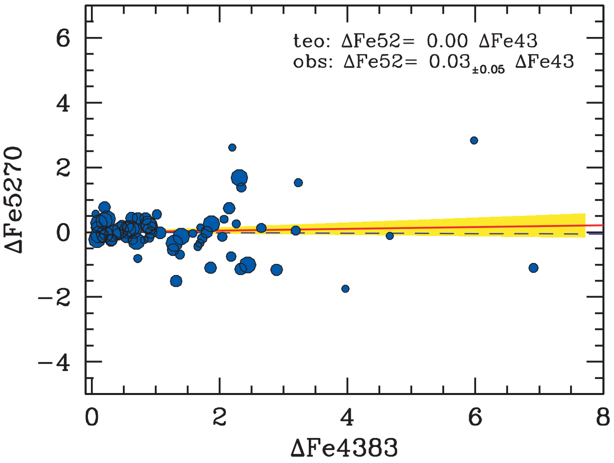

Figure 3. Envisaged Δ–Δ test among galaxy spectroscopic indices for the Buzzoni et al. (2009b, 2015) galaxy sample (see text for details). It is shown here for the illustrative case of Fe4383 (index x) and Fe5270 (index y). If we assume the source of the left–right index difference to be only of a stochastic nature, then no correlation would be expected between Δ Fe4383 and Δ Fe5270. A least-squares linear fit to the data, in the form of $\Delta y = \alpha \Delta x$, actually provides $\alpha = 0.03 \pm 0.05$ (solid line with the yellow fan marking the $\pm 1\sigma$ standard deviation of the slope estimator), fully consistent with a flat trend (dashed line), as expected for this case. As a guideline, the dot size in the plot is smaller for index measurements at farther radial distances from the galaxy centre.

3.2 *Ménage à trois*: Hβ, [O III]$_{5007}$ and Fe5015

The wavelength region of galaxy spectra around 5000 Å may be heavily prone to the effects of gas emission. In particular, the Hβ and Fe5015 strengths could be affected, the first resulting from the parallel action of stellar absorption and gas emission, the latter because of the possible [O III] 5007 Å appearance (see Fig. 4). This issue is of central relevance as, within the Lick system, the Hβ index is the most suitable for placing strong constraints on the age of unresolved stellar aggregates (e.g., Buzzoni et al. 1994; Bressan, Chiosi & Tantalo 1996; Vazdekis et al. 1996; Tantalo, Chiosi & Bressan 1998; Kobayashi & Arimoto 1999; Maraston & Thomas 2000; Trager et al. 2000; Thomas et al. 2005; Fusi Pecci et al. 2005; Sánchez-Blázquez et al. 2006b; Peletier et al. 2007, and many others) due to its close response to the temperature location of the main-sequence turn-off stars (Gorgas et al. 1993; Buzzoni 1995; Buzzoni et al. 2009a).

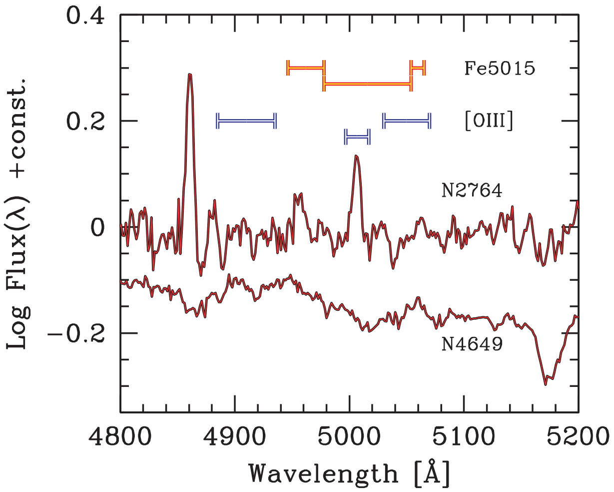

Figure 4. Nested configuration of the [O III]$_{5007}$ and Fe5015 indices. For each index, the two blue and red pseudo-continuum sidebands are reported, flanking the main feature window. Two representative spectra of active (NGC 2764) and quiescent (NGC 4649) elliptical galaxies, from our observed data base (Buzzoni et al. 2009b), are superposed on the index sketch, for comparison. In addition to the [O III] emission, note for NGC 2764 also a prominent Hβ emission at the nominal $\lambda\lambda$4861 Å.

A proper correction of this effect is not quite a straightforward task, especially when modest amounts of emission do not appear as surging features in the spectra and instead hide, making the absorption line depth artificially shallower. If uncorrected, this effect would bias age estimates towards older values. A first attempt to account for Hβ_e residual emission is due to González (1993), who assumed the [O III]$_{5007}$ index to be a confident proxy for Hβ correction. A simple scheme was devised for this, where the observed Balmer index was offset by $\Delta \mathrm{H}\,\beta = \mathrm{H}\,\beta_e = -0.7[\mathrm{O\,III}]_{5007}$ (González 1993). This approach relies on the fact that [O III] emission would be much more clearly recognizable than possibly hidden Hβ emission, and [O III] and Balmer emission do somewhat correlate as they ostensibly originate in the same regions of the galaxies. One has to note, however, that later attempts to settle the problem empirically (Carrasco et al. 1995; Trager et al. 2000; Kuntschner et al. 2006) reached puzzling conclusions, at odds with Gonzalez's predictions.

In a closer analysis, things may actually be much more entangled as: (i) apparent [O III] emission is partly at odds with Fe5015 absorption, as both indices partly overlap (see Fig. 4); (ii) fresh star formation could likely trigger both [O III] and Balmer emission but on different timescales (Moustakas, Kennicutt & Tremonti 2006; Buzzoni et al. 2015), and depend on oxygen abundance and ionization parameters (Osterbrock 1974; Pagel et al. 1979; Kewley & Dopita 2002). For all these reasons, the combined behaviour of the three indices, Hβ, [O III]$_{5007}$ and Fe5015, needs to be assessed self-consistently.

It is useful to start our analysis first with the [O III]$_{5007}$ versus Fe5015 interaction. Fig. 4 clearly shows that oxygen emission may be systematically underestimated as the [O III]$_{5007}$ continuum sidebands cannot account for Fe5015 absorption. This is especially true if one considers that Fe5015 strengthens in old stellar systems (Trager et al. 2000; Beuing et al. 2002; Ogando et al. 2008; Buzzoni et al. 2015) (see, for instance, the illustrative case of galaxy NGC 4649, also displayed in Fig. 4). Let us then compute the observed flux density within the [O III] and Fe5015 feature windows (of width w_O and w_{50}, respectively).

Recalling equations (2) and (9), and omitting the average overlined notation for flux density symbols, as well as the suffix on the oxygen index, for better legibility of the formulae, we have

$$\frac{f_O}{f_c} = \left(1 - \frac{[\mathrm{O\,III}]}{w_O}\right), \qquad \frac{f_{50}}{f_c} = \left(1 - \frac{\mathrm{Fe5015}}{w_{50}}\right). \tag{22}$$

Note that f_O is a sum of the genuine contribution of O emission plus the contribution of the *intrinsic* Fe5015 feature. Similarly, the intrinsic Fe5015 flux density (i.e., after fully removing O emission) is

$$\frac{f'_{50}}{f_c} = \left(1 - \frac{\mathrm{Fe5015}'}{w_{50}}\right), \tag{23}$$

where Fe5015′ stands for the corrected Fe5015 index strength. By definition, it must be

$$f'_{50}(w_{50} - w_O) = f_{50}\, w_{50} - f_O\, w_O \tag{24}$$

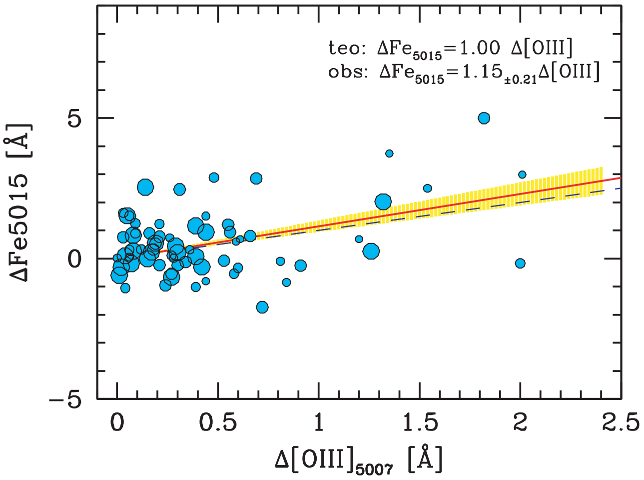

Figure 5. Δ–Δ correlation test, as for Fig. 3, for the [O III]$_{5007}$ and Fe5015 indices. The expected statistical prediction, according to equation (28) (dashed line), is well matched by the observations, which provide a fully consistent $\alpha = 1.15 \pm 0.21$ fitting line slope (solid line within a $\pm 1\sigma$ yellow fan), as reported in the top right of the plot.

so that, after matching equation (22),

$$\frac{f'_{50}}{f_c} = \left[\frac{w_{50}\left(1-\frac{\mathrm{Fe5015}}{w_{50}}\right) - w_O\left(1-\frac{[\mathrm{O\,III}]}{w_O}\right)}{(w_{50}-w_O)}\right]. \tag{25}$$

Combining equations (23) and (25) leads to

$$\mathrm{Fe5015}' = w_{50}\left(1-\frac{f'_{50}}{f_c}\right) = \frac{w_{50}}{w_{50}-w_O}\,(\mathrm{Fe5015} - [\mathrm{O\,III}])\,. \tag{26}$$

By replacing the corresponding width of each feature window (namely $w_O = 20$ Å and $w_{50} = 76.3$ Å, see Table 1), the intrinsic Fe5015 index can eventually be written explicitly in terms of the observed quantities as:

$$\mathrm{Fe5015}' = 1.36\;(\mathrm{Fe5015} - [\mathrm{O\,III}])\,. \tag{27}$$

For the Δ–Δ index distribution, if the same (intrinsic) value of Fe5015′ has to be expected for the galaxy's left and right sides, at fixed radial distances, then any difference in the observed Fe5015 index may be induced by a change in the [O III] emission. By simply differentiating equation (27), we obtain a straight positive correlation such as:

$$\Delta\mathrm{Fe5015} = \Delta[\mathrm{O\,III}]. \tag{28}$$

Again, when comparing with our data in Fig. 5, a least-squares solution for 68 selected points in total (after a 3σ clipping) provides a fully consistent slope value $\alpha = 1.15 \pm 0.21$.

Quite importantly, turning back for a moment to equation (27), one has to notice that when [O III] emission fades and Fe5015 tends to Fe5015′, then the [O III] index *does not vanish*. In fact, if we set Fe5015 = Fe5015′ in equation (26), we obtain:

$$[\mathrm{O\,III}]_{\mathrm{min}} = \frac{w_O}{w_{50}}\mathrm{Fe5015}' = 0.26\;\mathrm{Fe5015}'. \tag{29}$$

More generally, if some emission occurs, then $[\mathrm{O\,III}]' = [\mathrm{O\,III}] - [\mathrm{O\,III}]_{\mathrm{min}}$, and

$$[\mathrm{O\,III}]' = [\mathrm{O\,III}] - 0.26\;\mathrm{Fe5015}' \tag{30}$$

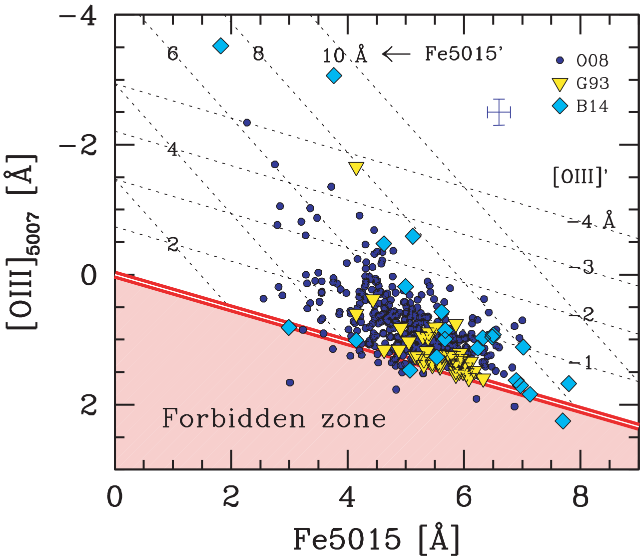

Figure 6. Observed (raw) [O III]$_{5007}$ versus Fe5015 index distribution for the Ogando et al. (2008) (solid dots), González (1993) (triangles) and Buzzoni et al. (2009b, 2015) (rhombi) samples of early-type galaxies. The forbidden zone in the index domain is shaded, according to equation (31), while a more general parametrization versus intrinsic Fe5015 and [O III]$_{5007}$ strength (primed indices in the plot) is displayed, following equations (27) and (31). An indicative error box for the observations is reported top right.

or

$$[\mathrm{O\,III}]' = 1.36\;[\mathrm{O\,III}] - 0.36\;\mathrm{Fe5015}, \tag{31}$$

which is in terms of the observed quantities. Equation (30) gives the locus in the Fe5015 versus [O III] plane for any intrinsic emission strength [O III]′.

By combining equations (26) and (30), an obvious self-consistency constraint implies that

$$\mathrm{Fe5015}' = \mathrm{Fe5015} - [\mathrm{O\,III}]'. \tag{32}$$

A graphical summary of our theoretical scheme is sketched in Fig. 6, where we compare the [O III] versus Fe5015 distribution for the galaxies of Table 2 with the observed distribution of an extended sample of 509 ellipticals from Ogando et al. (2008) and with the original bulk of 41 ellipticals from González (1993). The trend seems quite encouraging, and actually suggests an important property of ellipticals. Within the limits of the calibration of Ogando et al. (2008) (see, in particular, their tables 7 and 8), these data indicate that a substantial fraction of galaxies displays some residual oxygen emission (Sarzi et al. 2006; Papaderos et al. 2013). This important issue can be better assessed in Fig. 7, where we derive the distribution of the intrinsic emission [O III]′ as equation (31). The whole sample of 498 galaxies with available Fe5015 and [O III]$_{5007}$ indices leads to a mean index strength $\langle[\mathrm{O\,III}]'\rangle = -0.70 \pm 0.54$ Å, with an evident skewness towards enhanced [O III] emissions. As a reference, 16 objects out of 498 (3 per cent) in the figure display an intrinsic [O III] feature stronger than 2 Å, while for 107 galaxies (21 per cent) the [O III] emission exceeds 1 Å.

After disentangling the combined behaviour of [O III] emission and Fe5015 absorption, we are now in a better position to tune an Hβ correction scheme. Again, our Δ–Δ diagnostic plot may add useful hints for tackling the problem. The rationale, in this case, is that the observed $\Delta[\mathrm{O\,III}]_{5007}$ should directly trace the corresponding [O III]′ intrinsic change, via equation (30), providing the Fe5015′ strength is the same at symmetric distances from the galaxy centre. We could

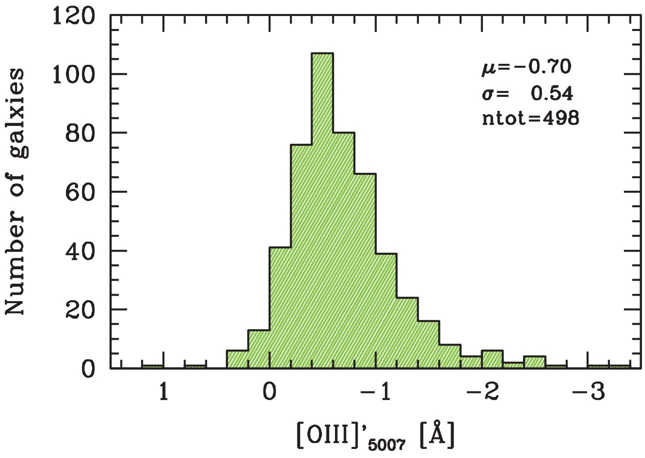

Figure 7. $[\mathrm{O\,III}]_{5007}$ distribution of the intrinsic (primed) index for the early-type galaxy sample of Ogando et al. (2008). A total of 498 galaxies with available $[\mathrm{O\,III}]_{5007}$ and Fe5015 observations are displayed. The [O III] observations have been corrected according to equation (31). On average, ellipticals display a weak residual gas emission with $\langle[\mathrm{O\,III}]'_{5007}\rangle = -0.70 \pm 0.54$ Å. For 21 per cent of the total sample, the intrinsic [O III] pseudo-equivalent width is in excess of 1 Å, while about 1/7 of these galaxies (16 out of 498) display striking (star-formation) activity, with $[\mathrm{O\,III}]'_{5007} \lesssim -2$ Å.

therefore probe the Δ Hβ data set for any possible correlation with the corresponding $\Delta[\mathrm{O\,III}]_{5007}$ output in a fully empirical way.

For this task, we divided the whole galaxy set of Table 2 (Sample A) into different sub-samples according to the activity level as traced by the overall spectral characteristics. In particular, we considered three reference samples. Sample B consists of the seven quiescent galaxies with no reported emission lines. Sample C includes the eight moderately active objects, marked with one asterisk in the table, which are reportedly emitting at least the [O II] 3727 Å feature. Finally, the five most active ellipticals (those marked with a double asterisk in Table 2) are included in Sample D. They display [O II] 3727 Å emission accompanied by the strongest [O III]′ index in Fig. 6. Our results are summarized in the four panels of Fig. 8. As usual, the fitting slope after 3σ data clipping is presented in Table 3 together with the mean of central corrected [O III] emission (from Buzzoni et al. 2015).

A firm important conclusion of our analysis is that there does not seem to be any striking correlation across the whole galaxy sample between Hβ and $[\mathrm{O\,III}]_{5007}$. A mild positive slope is found overall (Sample A, upper left-hand panel in Fig. 8), only marginally in excess of the flat-slope case ($\alpha = 0.0$–0.2). The flattening effect is clearly induced by the fraction of quiescent ellipticals (Sample B, upper right-hand panel), for which we even notice a slight anti-correlation ($\alpha \sim -0.2$). However, with increasing stellar activity, as in Sample C and D galaxies, there are hints of a change. Although with increased scatter and a much blurred trend, the data seem to point to a steeper slope α and, at least for Sample D (lower left-hand panel in the figure), our results nominally match the value in González (1993).

As a plain rule of thumb, the correction scheme of González (1993) fully holds for the most active strong-lined ellipticals, where [O III]′ emission roughly exceeds 2 Å. For intermediate cases (say for [O III]′ emission strength about 1 Å) a flatter slope ($\alpha \sim 0.3$–0.5) might be more appropriate, while a negligible Hβ correction ($\alpha \sim 0.1$) is required for weaker [O III] emission. As shown in Fig. 9,

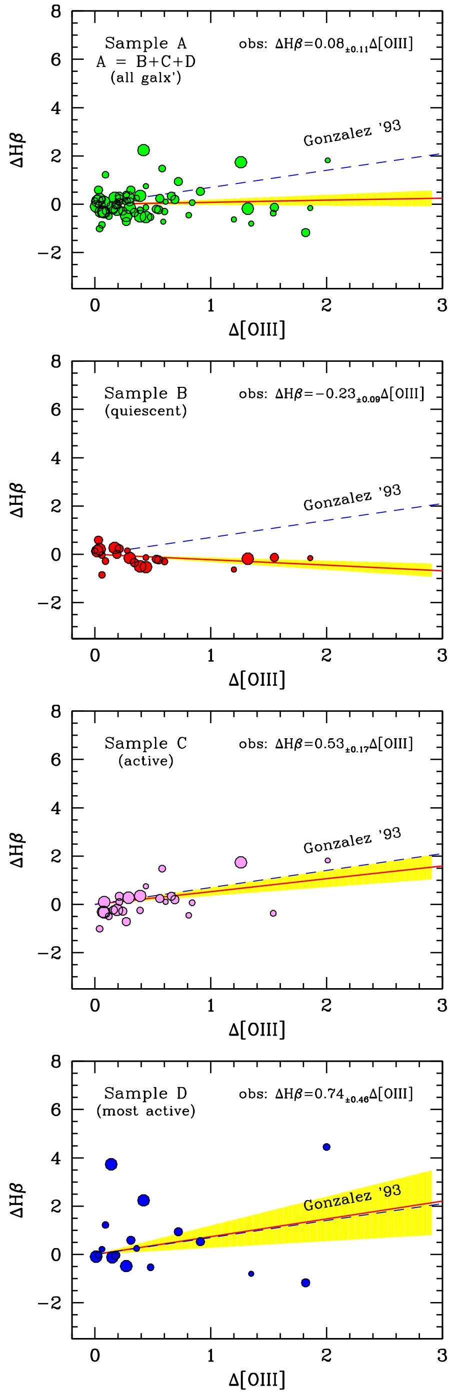

Figure 8. Δ–Δ correlation test, as for Fig. 3, for the $[\mathrm{O\,III}]_{5007}$ and Hβ indices in the adopted Buzzoni et al. (2009b, 2015) sample of early-type galaxies. The whole of Sample A, 20 objects (upper panel), is split into three groups (i.e., Samples B, C and D, from top to bottom) consisting, respectively of seven, eight and five galaxies with increasing gas emission activity. Groups have been assembled according to the asterisk ranking of Table 1, which combines the Bettoni & Buson (1987) empirical classification with the [O III] index strength in our observations. The dashed line, in each plot, marks the González (1993) Δ–Δ correction slope. Our least-squares fit is reported in the top right in each panel, and displayed (solid line) together with its corresponding ±1σ uncertainty (yellow fan). Our output is summarized in Table 3.

Table 3. Core [O III]′ emission strength and observed Δ Hβ versus Δ[O III] fitting slope.

Sample	⟨[O III]′⟩^{a}	α	n^b
A – All galaxies (20)	−1.1 ± 1.7	0.08 ± 11	68
B – Quiescent (7)	−0.15 ± 74	−0.23 ± 9	23
C – Intermediate active (8)	−0.67 ± 49	0.53 ± 17	25
D – Most active (5)	−3.1 ± 2.3	0.74 ± 46	17

Notes. ^{a}Mean core [O III]′ index, in Å, as Buzzoni et al. (2015). ^{b}Number of available pairs of points in the α fit.

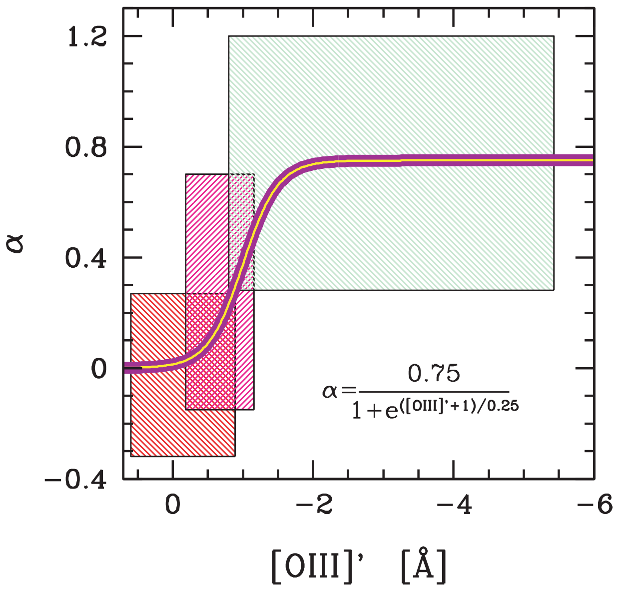

Figure 9. Devised correction scheme for Hβ in the form of a logistic curve versus intrinsic [O III]′ emission, from equation (33). The quiescent, active and most active galaxy samples of Fig. 8 are sketched by the three shaded boxes, with [O III]′ mean central values and α error bars from Table 3.

a logistic curve could be adopted as a convenient analytical fit of this scheme, such as:

$$\alpha = \frac{0.75}{1 + \mathrm{e}^{k}}, \tag{33}$$

with $k = ([\mathrm{O\,III}]' + 1)/0.25$, and [O III] emission assumes, of course, negative values. The corrected Hβ index is, therefore:

$$\mathrm{H}\,\beta_{\mathrm{corr}} = \mathrm{H}\,\beta_{\mathrm{obs}} - \mathrm{H}\,\beta_{e} = \mathrm{H}\,\beta_{\mathrm{obs}} - \alpha\,[\mathrm{O\,III}]'. \tag{34}$$

3.3 Mg$_1$ + Mg*b* = Mg$_2$?

The prominent magnesium feature about 5200 Å is by far the most popular target in optical spectroscopy of elliptical galaxies and other old stellar systems. As explored in full detail by Mould (1978) from a theoretical point of view, this feature is a blend of both the atomic contribution of the Mg*b* triplet at 5178 Å, and the (1,1) $A^2\Pi\, X^2\Sigma^+$ vibrational band head of the MgH molecule. This transition of magnesium hydride has a dissociation energy of 1.34 eV (Coelho et al. 2005, from Huber & Herzberg 1979 data), a much lower threshold than the first-ionization potential of 7.65 eV for atomic Mg. As a consequence, Mg*b* absorption tends to prevail in warmer stars (type F-G), while it accompanies the surging MgH absorption of the much cooler temperature regime of K-M stars. In addition, the relatively more flimsy structure of the molecule makes MgH very sensitive to stellar luminosity class (Buzzoni et al. 2001), as gravity acts on the electron pressure of the stellar plasma and slightly modulates the dissociation energy threshold. This dependence, however, is severely tackled by the intervening appearance of TiO bands among M-type stars, which substantially affect the pseudo-continuum level (see, for instance fig. 5 in Buzzoni et al. 1992; Tantalo & Chiosi 2004).

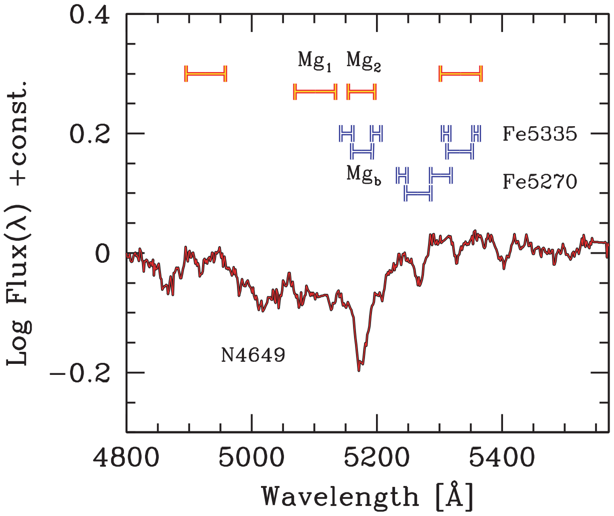

Figure 10. Illustrative sketch of the Mg index set, and the two Fe5270 and Fe5335 indices. For each index, the blue and red sidebands are marked, flanking the relevant feature window. The nested configuration of the Mg*b*, Fe5335 and Mg$_2$ indices is very evident, as discussed in the text. The representative spectrum of the elliptical galaxy NGC 4649 (from the Buzzoni et al. 2009b data) is superposed for comparison.

The magnesium complex is sampled by three Lick indices, namely Mg$_1$, Mg$_2$ and Mg*b*. The strategy is for Mg$_2$ to somewhat bridge the other two, with Mg$_1$ especially suited to probe the molecular contribution, and the Mg*b* index better tuned for the atomic triplet (see Fig. 10). Within this configuration, Mg$_2$ shares a feature window with Mg*b*, and its pseudo-continuum windows with the Mg$_1$ index. Mg*b* aims to recover the genuine atomic contribution by setting its pseudo-continuum level about the Mg$_1$ bottom (see again Fig. 10 for an immediate sketch).

As discussed in the previous section, we can further expand our scheme to assess in a more straightforward way the Mg$_2$–Mg*b*–Mg$_1$ index entanglement. First of all, as both Mg$_2$ and Mg$_1$ are expressed in magnitudes and Mg*b* in Å, it is convenient to recall the basic relations of equations (3) and (4) and write

$$\begin{cases} f_2/f_c &= 10^{-0.4\,\mathrm{Mg}_2} \\ f_1/f_c &= 10^{-0.4\,\mathrm{Mg}_1} \\ f_b/f_1 &= (1 - \mathrm{Mg}b/w_b)\,. \end{cases} \tag{35}$$

We can also combine the last two equations above to obtain

$$\frac{f_b}{f_c} = \left(\frac{f_b}{f_1}\right)\left(\frac{f_1}{f_c}\right) = \left(1 - \frac{\mathrm{Mg}b}{w_b}\right)\, 10^{-0.4\,\mathrm{Mg}_1}. \tag{36}$$

Quantities f_2,f_1 and f_b in the above equations refer to the flux density of the Mg$_2$, Mg$_1$ and Mg*b* feature windows, respectively, and w_b is the width of the Mg*b* feature window. For Mg$_1$ and Mg$_2$, this flux is normalized to the same pseudo-continuum, f$_c$, while the f$_1$ bottom level can also be seen as a proxy of the Mg*b* pseudo-continuum.

Likewise for equation (24), also for Mg, we can write:

$$f_2\, w_2 = f_1\,(w_2 - w_b) + \left(\frac{f_b}{f_1}\right)\, f_1\, w_b, \tag{37}$$

with $w_2 = 42.5$ Å and $w_b = 32.5$ Å (from Table 1), which are the widths of the Mg_2 and Mg*b* feature windows, respectively. By matching equations (35), (36) and (37) and taking logarithms, after a little arithmetic, we get the final form that links the three indices:

$$\mathrm{Mg}_2 - \mathrm{Mg}_1 = -2.5 \log\left(1 - \frac{\mathrm{Mg}b}{w_2}\right) + k. \qquad (38)$$

In the equation, we left a fine-tuning offset (k) to account for the little approximation we made in equation (35) for f_1 to be an exact proxy of the Mg*b* pseudo-continuum level. It is interesting to verify empirically the invariance of the function

$$\phi(\mathrm{Mg}) = \mathrm{Mg}_2 - \mathrm{Mg}_1 + 2.5 \log\left(1 - \frac{\mathrm{Mg}b}{w_2}\right) - k. \qquad (39)$$

Again, Ogando et al. (2008) together with the galaxy data base of Trager et al. (1998) provide us with an excellent reference tool. Our results are summarized in the two panels of Fig. 11. As predicted, the lack of any drift of $\phi(\mathrm{Mg})$ versus Mg_2 (and versus Mg_1 and Mg*b*, as well) indicates that no residual dependency has been left unaccounted for in our analysis. By searching for the least-squares fit to the data, we also get an empirical estimate for the fine-tuning offset, that is $k = 0.03$ mag. Providing we observe two indices, equation (38) allows us to secure the third one within a ~1.5 per cent internal accuracy.[2]

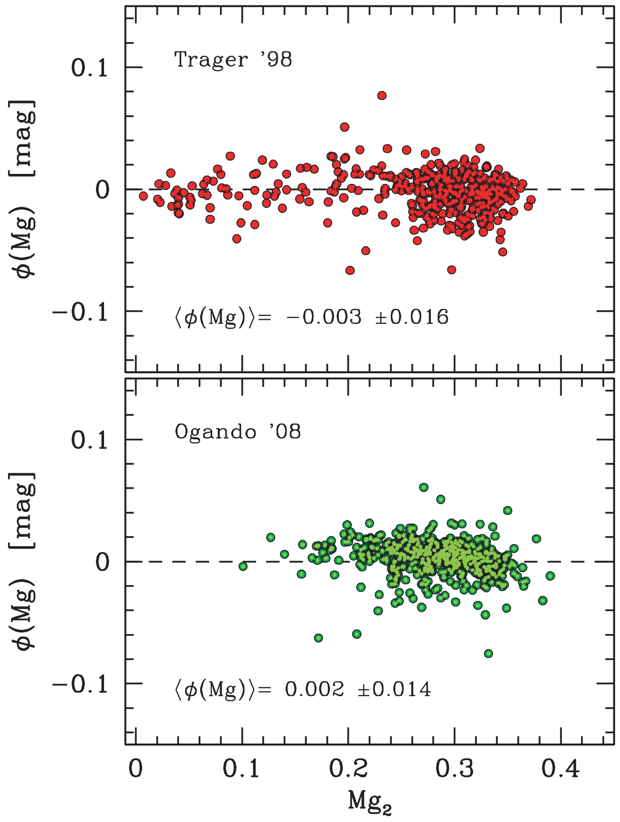

Figure 11. Empirical check of the expected relationship among the three popular Mg indices sampled by the Lick system. The synthesis function $\phi(\mathrm{Mg})$ of equation (39) has been scrutinized for the two extended early-type galaxy samples of Trager et al. (1998) (406 galaxies with complete Mg_1, Mg_2 and Mg*b* data, see upper panel), and Ogando et al. (2008) (481 galaxies, lower panel). The match with both samples allowed us to obtain the fine-tuning offset in the theoretical relationship, $k = 0.03$ mag. After applying the offset, notice for both plots the lack of any drift in the point distribution, a feature that ensures the correct parametrization of our theoretical relationship. In addition, the point scatter around the zero line indicates that an index mutual relationship can be obtained within a ~1.5 per cent internal accuracy.

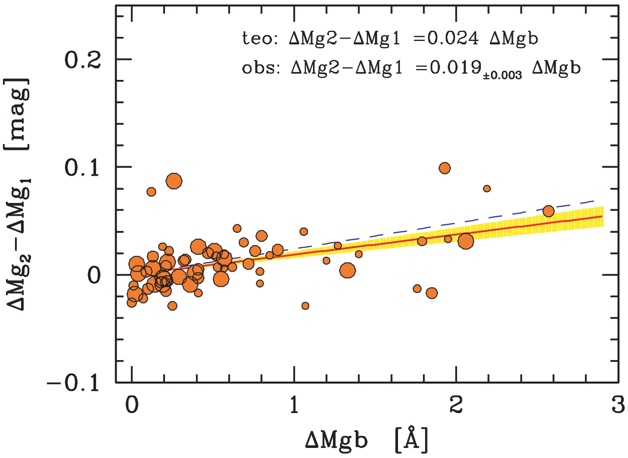

Figure 12. Δ–Δ correlation test, as for Fig. 3, for the Mg index complex. The ΔMg_1, ΔMg_2 and Δ Mg*b* variation across the Buzzoni et al. (2009b, 2015) galaxy sample of Table 2 is probed in terms of the expected relationship from equation (40) (dashed line in the plot). Our least-squares fit is reported at the top right, and displayed (solid line) together with its corresponding $\pm 1\sigma$ statistical uncertainty (yellow fan).

A further check can be carried out in terms of our Δ–Δ test. By differentiating equation (38), and considering that, in general, Mg*b* $\ll w_2$, we obtain:

$$\mathrm{dMg}_2 - \mathrm{dMg}_1 \simeq \frac{1}{w_2}\,\frac{\mathrm{dMg}b}{(1 - \mathrm{Mg}b/w_2)} \approx 0.024\,\mathrm{dMg}b. \qquad (40)$$

The theoretical relationship is probed in Fig. 12 with our galaxy sample of Table 2. The usual least-squares fit for 66 points provides a value of the slope: $\alpha = 0.019 \pm 0.003$.

3.3.1 The $[\mathrm{N\,I}]_{5199}$ hidden bias

As for the $[\mathrm{O\,III}]_{5007}$ perturbing emission to the Fe5015 index, also for the Mg*b* index one may expect a shifty, and mostly neglected, bias from overlapping gaseous emission lines. This is the [N I] forbidden doublet at 5198/5200 Å (hereafter $[\mathrm{N\,I}]_{5199}$), a somewhat ominous weak feature that characterizes the spectra of LINER galaxies (see appendix 4 in Osterbrock 1974), including ellipticals, either due to residual star formation activity (Sarzi et al. 2006; Cappellari et al. 2011), or simply supplied by the post-asymptotic giant branch stellar component (Kaler 1980; Ferland et al. 2012; Kehrig et al. 2012; Papaderos et al. 2013).

Goudfrooij & Emsellem (1996) discussed in some detail the perturbing effect of $[\mathrm{N\,I}]_{5199}$ on the computed Mg*b* index in the spectra of elliptical galaxies. Unlike the $[\mathrm{O\,III}]_{5007}$ versus Fe5015 interplay, the $[\mathrm{N\,I}]_{5199}$ emission *positively* correlates with the affected Mg*b* as [N I] luminosity enhances the pseudo-continuum level in the red sideband of Mg*b* (see Fig. 10), thus leading to a stronger index.

A simple correction scheme can be devised to determine the $[\mathrm{N\,I}]_{5199}$ bias relying only on the third relation of equation (35)

---

[2] Note that, for vanishing values of Mg*b*, as in low-metallicity stellar populations, equation (38) further simplifies, as its right-hand term can be usefully approximated by the linear term of its series expansion, i.e., $[k + 1.09\,(\mathrm{Mg}b/w_2)] \sim 0.03\,(\mathrm{Mg}b + 1)$. In this case, the Mg indices straightforwardly relate as $\mathrm{Mg}_2 \simeq \mathrm{Mg}_1 + 0.03\,(\mathrm{Mg}b + 1)$.

(and, again, assuming f_1 as the reference Mg*b* pseudo-continuum flux density). By taking logarithms we have:

$$\ln\left(1 - \frac{\mathrm{Mg}b}{w_b}\right) = \ln(f_b) - \ln(f_1). \tag{41}$$

Again, considering that Mg*b* $\ll w_b$, the left-hand term of the equation can be approximated by $-(\mathrm{Mg}b/w_b)$ so that, by differentiating with respect to f_1, we have

$$\frac{\mathrm{dMg}b}{w_b} \simeq \frac{\mathrm{d}f_1}{f_1}. \tag{42}$$

If [N I]$_{5199}$ emission appears, then a supplementary flux F_N is added to the Mg*b* pseudo-continuum, and its reference flux density changes by $\mathrm{d}f_1 = F_N/W_b$, where $W_b = 33.7$ Å from Table 1. As, by definition, the [N I] equivalent width[3] is $[\mathrm{N\,I}]_{5199} \simeq -F_N/f_1$, equation (42) can eventually be rearranged in its final form:

$$\mathrm{dMg}b = -[\mathrm{N\,I}]_{5199}\left(\frac{w_b}{W_b}\right) \simeq -0.96\,[\mathrm{N\,I}]_{5199}. \tag{43}$$

Our result nicely compares with that of Goudfrooij & Emsellem (1996), who gave a cruder analytical estimate of the effect: $\mathrm{dMg}b \simeq -1.1\,[\mathrm{N\,I}]_{5199}$.

The extended galaxy data base of Ogando et al. (2008) allows a further independent assessment of the [N I]$_{5199}$ bias among elliptical galaxies. In this regard, we set up a simple test to compare the observed Mg*b* index for the entire galaxy data set with the corresponding predicted output from equation (38). Galaxies with intervening [N I] emission are expected to display (on average) a stronger than predicted Mg*b* index, and one could envisage detecting this signature in the residual distribution of the observed–computed (O-C) index.

To get cleaner information, we restricted our analysis only to the galaxy sub-sample with stronger and poorer [O III]$_{5007}$ emission, assuming [O III]$_{5007}$ to be also a confident proxy for [N I]$_{5199}$ activity (Osterbrock 1974). According to the $[\mathrm{O\,III}]'_{5007}$ distribution of Fig. 7, we therefore selected a sample of 41 active galaxies with $[\mathrm{O\,III}]'_{5007} < -1.5$ Å emission, to be compared with a group of 275 objects with average or less than average emission ($[\mathrm{O\,III}]'_{5007} > -0.7$ Å). For each galaxy with observed Mg$_2$ and Mg$_1$ indices, we then computed the corresponding Mg*b*, via equation (38) (by setting $k = 0.03$), and compared it with the observed entry in the catalogue. The output distribution for the active and quiescent galaxy samples is displayed in Fig. 13. According to equation (43), the O-C residuals have been directly converted into a fiducial [N I]$_{5199}$ emission strength, as shown in the upper *x*-axis scale of the figure. Within the uncertainty of our theoretical procedure, just a glance at Fig. 13 confirms the lack of any [N I] emission among quiescent galaxies ($\langle[\mathrm{N\,I}]_{5199}\rangle = +0.15 \pm 0.03$ Å, on average), while there is a weak but significant ($>3\sigma$) activity, in contrast, for active systems, with $\langle[\mathrm{N\,I}]_{5199}\rangle = -0.29 \pm 0.11$ Å. Interestingly, the [N I]/[O III] ∼0.3/1.5 observed ratio for the active sub-sample matches the corresponding empirical figure for LINER galaxies, as suggested by Goudfrooij & Emsellem (1996, see table 1 therein).

3.4 Spectral duality of Fe5335

Due to wavelength oversampling, along the Lick-index sequence it may even happen that individual spectral features are accounted twice, being included in the pseudo-continuum windows of other indices. One relevant case is the Fe5335 index, which is fully inside the (red) pseudo-continuum window of both the Mg$_2$ and Mg$_1$ indices. In addition, it also entirely shares its own red pseudo-continuum with the blue side-window of Fe5270 (see, again, Fig. 10). Evidently, this makes both the Fe5270 and the Mg indices somewhat correlate with the Fe5335 strength. To explore this effect, let us start first with the simpler case of Fe5335–Fe5270 entanglement.

According to Table 1, the Fe5270 pseudo-continuum is sampled along a total of 47.5 Å (i.e., red+blue side-windows, W_{52}), whose 11.3 Å are shared with the Fe5335 red sideband (W_{53}^{red}). The total side-windows for Fe5335 (i.e., $W_{53} = W_{53}^{\mathrm{red}} + W_{53}^{\mathrm{blue}}$) amount to 21.2 Å, and both features are sampled within similar wavelength windows (w_{52} and w_{53}) of 40 Å each. From equation (2) and taking logarithms, for Fe5270 we have:

$$\ln\left(1 - \frac{\mathrm{Fe5270}}{w_{52}}\right) = \ln(f_{52}) - \ln(f_{52}^{c}). \tag{44}$$

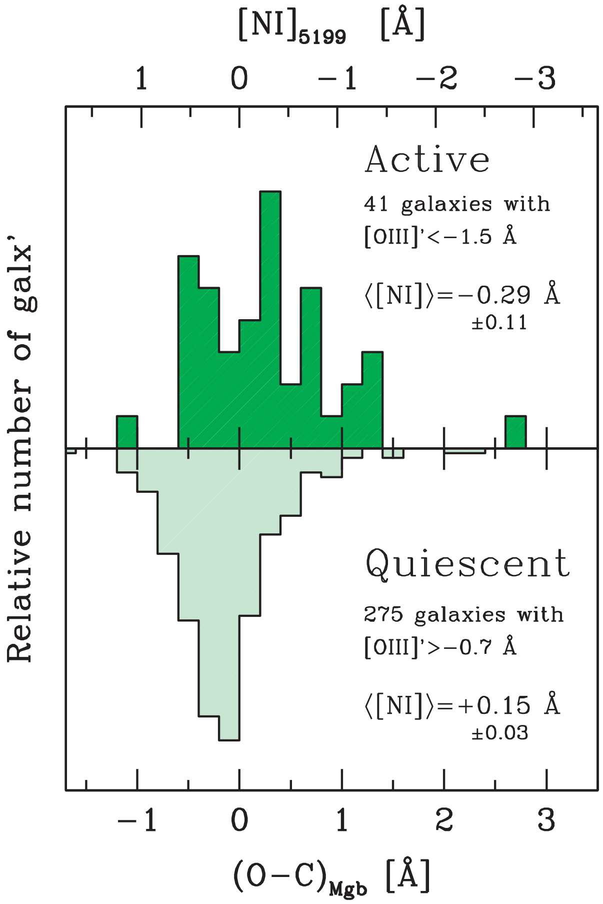

Figure 13. Inferred distribution of the hidden [N I]$_{5199}$ gas emission in the Ogando et al. (2008) galaxy sample. For intervening [N I] emission, the Mg*b* index is expected to be enhanced, on average, by the amount of equation (43) with respect to its theoretical figure from equation (38). This excess (in the sense observed–computed, see lower *x*-axis), and the related [N I] strength (upper *x*-axis) is probed by contrasting the sub-sample of 41 active galaxies (as traced by explicit [O III] emission stronger than 1.5 Å, as in the upper histogram) with the population of 275 quiescent galaxies with vanishing [O III] (see the lower histogram). See text for a discussion.

---

[3] Note that we maintain a *negative* notation for *emission* lines. This explains the minus sign in the relevant equations throughout our discussion.

As we are dealing with a weak absorption line (so that $\mathrm{Fe5270}/w_{52} \ll 1$) the left-hand term of the equation can be approximated by $-(\mathrm{Fe5270}/w_{52})$. By differentiating,

$$\left(\frac{\mathrm{dFe5270}}{w_{52}}\right) = \frac{\mathrm{d}f_{52}^c}{f_{52}^c} - \frac{\mathrm{d}f_{52}}{f_{52}}. \tag{45}$$

A similar notation holds for Fe5335, too. Any change (for whatever reason) in the f_{53}^c flux density, would therefore reverberate into a change in the Fe5270 and Fe5335 strengths as well, so that

$$\left(\frac{\mathrm{dFe5270}}{w_{52}}\right) = \frac{\mathrm{d}f_{52}^c}{f_{52}^c} \sim \frac{\mathrm{d}f_{53}^c}{f_{53}^c}\,\frac{W_{53}^{\mathrm{red}}}{W_{52}} \sim \left(\frac{\mathrm{dFe5335}}{w_{53}}\right)\left(\frac{W_{53}^{\mathrm{red}}}{W_{52}}\right), \tag{46}$$

or

$$\mathrm{dFe5270} = \left(\frac{11.3}{47.5}\right)\,\mathrm{dFe5335} = 0.238\,\mathrm{dFe5335}. \tag{47}$$

The chance for Fe5335 to entangle Fe5270 depends on the probability of any random change in the Fe5335 index bands affecting the wavelength range in common with the Fe5270 pseudo-continuum. This can be be estimated to be of the order of $W_{53}^{\mathrm{red}}/(W_{53} + w_{53}) \sim 11.3/61.2 = 18$ per cent. Therefore, the probability for no entanglement at all between the two indices is 82 per cent. By accounting for these figures, the *average* expected relationship between Fe5270 and Fe5335 eventually results in:

$$\begin{aligned}\mathrm{dFe5270} &= (0.238 \times 0.18) + (0 \times 0.82)\,\mathrm{dFe5335}\\ &= 0.043 \pm 0.091\,\mathrm{dFe5335}.\end{aligned} \tag{48}$$

This value has to be compared with the Δ–Δ test as displayed in the upper panel of Fig. 14. From our data (66 points in total) we obtain $\alpha = 0.059 \pm 0.068$.

Quite importantly, note that equation (48) cannot be simply reversed, becaue of the impact of the overlapping window on the Fe5335 strength (because $W_{53} \neq W_{52}$). By reversing the indices in equation (46), we have:

$$\left(\frac{\mathrm{dFe5335}}{w_{53}}\right) = \frac{\mathrm{d}f_{53}^c}{f_{53}^c} \sim \frac{\mathrm{d}f_{52}^c}{f_{52}^c}\,\frac{W_{53}^{\mathrm{red}}}{W_{53}} \sim \left(\frac{\mathrm{dFe5270}}{w_{52}}\right)\left(\frac{W_{53}^{\mathrm{red}}}{W_{53}}\right), \tag{49}$$

or

$$\mathrm{dFe5335} = \left(\frac{11.3}{21.2}\right)\,\mathrm{dFe5270} = 0.533\,\mathrm{dFe5270}. \tag{50}$$

This interaction has a probability of the order of $W_{53}^{\mathrm{red}}/(W_{52} + w_{52}) \sim 11.3/87.5 = 13$ per cent, so that, like equation (48), the eventual relationship, by reversing the indices in a Δ–Δ test becomes:

$$\begin{aligned}\mathrm{dFe5335} &= (0.533 \times 0.13) + (0 \times 0.87)\,\mathrm{dFe5270}\\ &= 0.07 \pm 0.18\,\mathrm{dFe5270}.\end{aligned} \tag{51}$$

Again, this relationship can be probed by means of our Δ–Δ test, as shown in the lower panel of Fig. 14, suggesting $\alpha = 0.19 \pm 0.22$.

For the $\mathrm{Mg_2}$– (or $\mathrm{Mg_1}$–) Fe5335 entanglement, we can proceed in a similar way, depending on whether a change occurs in the feature or in the sideband windows of the Fe I index. According to Table 1, the $\mathrm{Mg_2}$ (or $\mathrm{Mg_1}$) pseudo-continuum is sampled along a total of $W_2 = 127.5$ Å. Of these, 40 and 21.2 Å are shared, respectively, with the feature (w_{53}) and the sidebands (W_{53}) of the Fe5335 index.

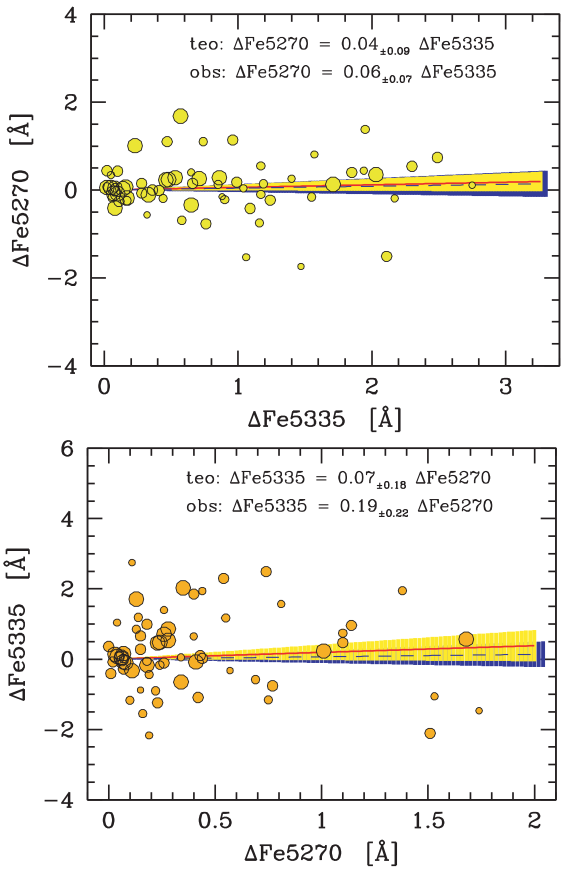

Figure 14. Δ–Δ correlation test, as for Fig. 3, for the Fe5270 and Fe5335 indices. The low correlation between index variation, as predicted by equations (48) and (51) (dashed lines in the two plots, with their corresponding ±1σ Bayesian uncertainties, the blue fans) is consistently summarized by our observing test on the galaxy sample of Table 2 (solid lines with their corresponding ±1σ statistical uncertainties, the yellow fans). See text for a discussion.

By recalling that $\mathrm{Mg_2}$ (and $\mathrm{Mg_1}$) are expressed in magnitude, the equivalent of equation (46), for an intervening change in the Fe5335 pseudo-continuum flux, becomes

$$\mathrm{dMg_2} \sim \frac{\mathrm{d}f_2^c}{f_2^c} \sim \frac{\mathrm{d}f_{53}^c}{f_{53}^c}\,\frac{W_{53}}{W_2} \sim \left(\frac{\mathrm{dFe5335}}{w_{53}}\right)\left(\frac{W_{53}}{W_2}\right), \tag{52}$$

which leads to

$$\mathrm{dMg_2} = \left(\frac{21.2}{40 \times 127.5}\right)\,\mathrm{dFe5335} = +0.0042\,\mathrm{dFe5335}. \tag{53}$$

This outcome has a probability of the order of $W_{53}/(W_{53} + w_{53}) \sim 21.2/61.2 = 35$ per cent.

On the other hand, any change in the Fe5335 feature window will affect the $\mathrm{Mg_2}$ ($\mathrm{Mg_1}$) strength by

$$\mathrm{dMg_2} \sim \frac{\mathrm{d}f_2^c}{f_2^c} \sim \frac{\mathrm{d}f_{53}}{f_{53}}\,\frac{w_{53}}{W_2} \sim -\left(\frac{\mathrm{dFe5335}}{w_{53}}\right)\left(\frac{w_{53}}{W_2}\right). \tag{54}$$

By replacing the relevant quantities, in this case we have

$$\mathrm{dMg_2} = -\left(\frac{1}{127.5}\right)\,\mathrm{dFe5335} = -0.0078\,\mathrm{dFe5335}, \tag{55}$$

with a probability of $w_{53}/(W_{53} + w_{53}) \sim 40/61.2 = 65$ per cent. Therefore, if a random process (of whatever origin) changes Fe5335, then the weighted average of equations (53) and (55) eventually

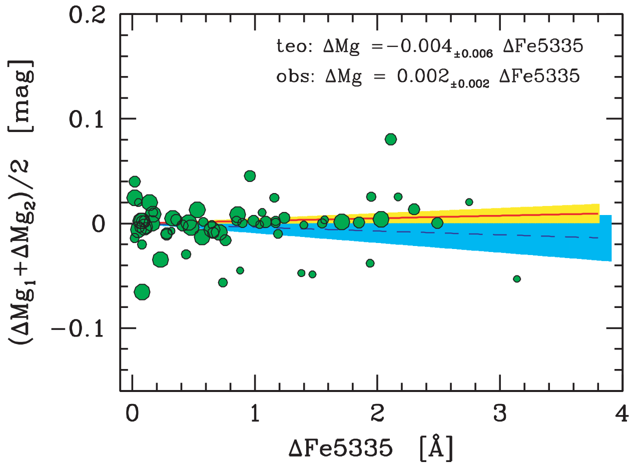

Figure 15. Δ–Δ correlation test, as for Fig. 3, for the Fe5335 and Mg indices. The observed relationship for Mg_1 and Mg_2 is averaged, to give a cleaner view of the effect. In spite of the *average* low correlation, as predicted by equation (56) (dashed line), notice the important Bayesian uncertainty (blue fan in the plot, tracing the $\pm 1\sigma$ uncertainty), which makes the bias effect of Mg–Fe5335 entanglement possibly of non-negligible impact on individual galaxies.

provides us with the expected relationship for Mg_2 (and similarly, for Mg_1, as well):

$$\mathrm{dMg}_2 = \mathrm{dMg}_1 = -0.0036 \pm 0.0057\,\mathrm{dFe5335}. \qquad (56)$$

Our theoretical output is probed in Fig. 15. The $\Delta\mathrm{Mg}_1$ and $\Delta\mathrm{Mg}_2$ versus ΔFe5335 variations are averaged to give a cleaner display of the effect. Observations actually confirm the nearly vanishing relationship across the whole galaxy sample, making the expected impact of a random change of Fe5335 on Mg indices negligible.

On the other hand, if a change in the Fe5335 feature occurs as a result of a genuine (selective) variation of Fe abundance, then only equation (55) has to be taken as a reference. Although small, the induced bias on Mg_2 (and Mg_1) may be an issue in this case, especially if we aim to investigate the [α/Fe] ratio in a galaxy sample carefully. In fact, any stronger Fe5335 index would induce, by itself, a shallower Mg index.

3.5 Mr Iron, I suppose...

About half of the total Lick indices are meant to trace iron as a main elemental contributor to the index feature. The ominous presence of weak (i.e., unsaturated) absorption lines of Fe I and Fe II in the optical/ultraviolet wavelength region is, of course, a well-established property of stellar spectra (e.g., Pagel 1997), which can be exploited by high-resolution spectroscopy to set up the linear branch of the spectral curve of growth, thus leading to an accurate measure of the elemental abundance. This figure is usually taken as an empirical proxy of stellar metallicity, generally by assuming iron to scale according to all the other metals. In the same way, also *UBV* broad-band photometry may rely on the blanketing effect, mainly driven by the iron contribution, to constrain stellar metallicity (e.g., Sandage 1969; Golay 1974).

In low-resolution spectroscopy or narrow-band photometry, as for the Lick indices, however, such a huge number of low-strength Fe lines may reveal a quite tricky feature, as iron markers actually come heavily blended with other elements. The potential drawback was emphasized, at least in a qualitative way, in earlier works dealing with the Lick-system assessment (Burstein et al. 1984; Faber et al. 1985; Gorgas et al. 1993; Worthey et al. 1994, among others). This analysis was taken further by Tripicco & Bell (1995), Worthey (1996), Trager et al. (1998) and Serven, Worthey & Briley (2005), urging in some cases a revision of the index label, as for the original Fe4668 index (Worthey 1996; Trager et al. 1998), now redefined as $\mathrm{C}_2$4668 according to the real prevailing contribution in the evolutionary context of old stellar populations, as in elliptical galaxies.

The Trager et al. (1998) revision process has been intentionally left at the highest conservative level, likely to avoid any massive re-definition of the original index set. However, we want to retake here some arguments of Worthey's (1996) preliminary analysis to show that, at least for some relevant cases dealing with *bona fide* Fe features, an important update effort seems yet to impose. We will defer this delicate task to a forthcoming paper discussing here, just as an illustrative exercise, the index Fe4531.

3.5.1 *Absolute and net index sensitivity*

The main rationale for the Lick-index set up (Worthey et al. 1994) is to catch all the prominent absorption features in the optical spectra of late-type stars (type G-K). This uniquely requires a feature to be easily recognized at a ∼8.5 Å (FWHM) resolving power. If a blend could be envisaged for a feature, the latter is tacitly assumed to be named after the element contributing with the deepest line, as recognized from the list of theoretical atomic transitions (e.g., Piskunov et al. 1995; Smith et al. 1996; Kupka et al. 1999). The deepest line also defines the feature centroid, which is reported in the original table 1 of Worthey et al. (1994). There is no special requirement for the two index sidebands when sampling a nearby pseudo-continuum, other than being suitably feature-free and sufficiently extended in wavelength so as to be insensitive to stellar velocity dispersion broadening (Worthey et al. 1994).

So, while the main focus is on the feature prominence, that is on a feature's *absolute* sensitivity to the leading chemical element, one should not neglect that it is the index net sensitivity (that is, by netting the feature sensitivity to a given element with the impact of the latter on the pseudo-continuum bands, too) that eventually sets the real index response to a given chemical species.

Like Serven et al. (2005), to explore this important point we performed a test by probing the spectral wavelength region around the Fe4531 feature in the high-resolution spectra of two reference templates for old stellar populations, namely the Sun (type G2V, seen at $R \sim 350\,000$ resolving power) and the star Arcturus (type K1.5 III, observed at $R \sim 80\,000$). For our analysis we relied on the SPECTROWEB 1.0 interactive data base of spectral standard star atlases (Lobel 2007, 2008, 2011). The web program interface allows an accurate fit of the observed spectra of these stars, supplying a detailed identification of all the chemical species with absorption features within the wavelength range (feature plus pseudo-continuum windows) of the Lick Fe4531 index.

The sensitivity of both the feature and the continuum windows to the first 40 most important absorbers has been quantified by summing all the relevant line depths [$d = 1 - I(\lambda)/I_c(\lambda)$] from the high-resolution spectrum. As we are always dealing with weak (i.e., unsaturated) lines, one could assume, with sufficient accuracy, the equivalent width to scale simply with the line depth. So, a measure of the absorbing strength of element X (disregarding its different

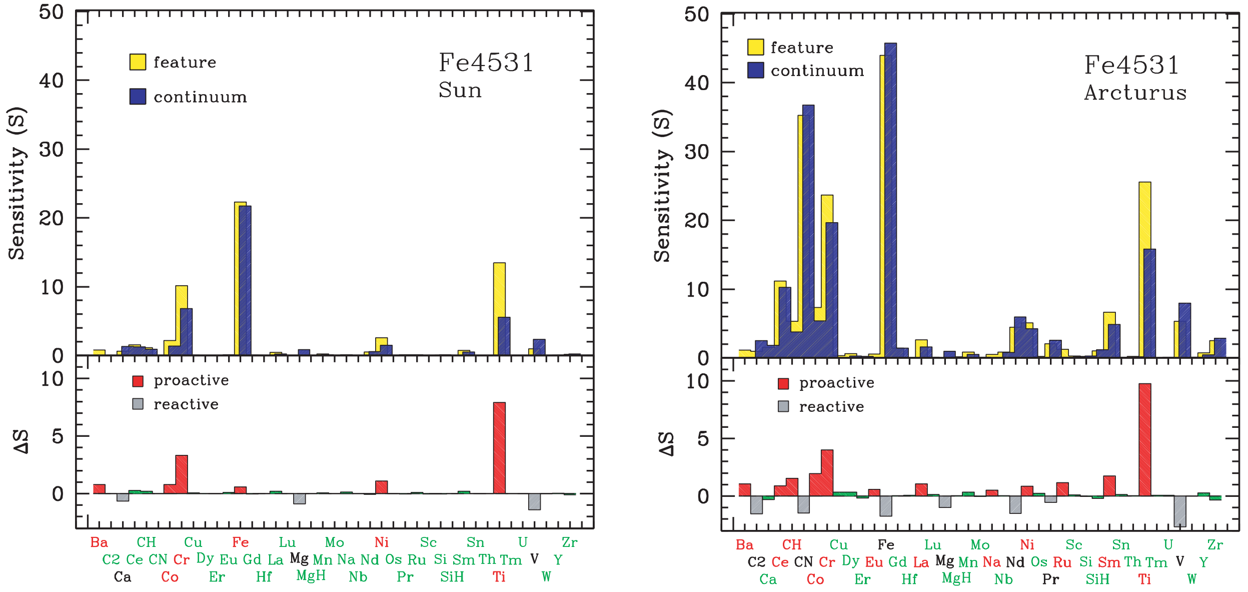

Figure 16. Fe4531 index sensitivity to the 40 most prominent chemical elements (as sequenced in the x-axis, disregarding their ionization states) in the Sun (left-hand panel) and Arcturus (right-hand panel) spectra. In both panels, the yellow histograms refer to the elemental contribution ($\mathcal{S}^f_X$) to the *feature* window, according to the definition of equation (57), while the blue histograms are for the elemental contribution ($\mathcal{S}^c_X$) to the flanking pseudo-continuum index sidebands, according to equation (58). The *net* contribution to the index strength ($\Delta\mathcal{S}_X$), from equation (59), is displayed in the lower plots, where proactive elements are displayed in red and reactive elements in grey. Note the leading role of titanium and the reactive action of vanadium and magnesium. See text for a full discussion.

ionization states) in the feature window of the index (of width w, from Table 1) can be written as:

$$\mathcal{S}^f_X = \sum^w d_x . \tag{57}$$

The same can be done for the pseudo-continuum sensitivity to the corresponding element:

$$\mathcal{S}^c_X = \left(\frac{w}{W}\right) \sum^W d_x , \tag{58}$$

where the width W comes again from Table 1. As, in general, $w \neq W$, in the latter case $\mathcal{S}^c_X$ should be normalized by a factor (w/W) to compare consistently with $\mathcal{S}^f_X$, as displayed in equation (58).

Clearly, the *net* sensitivity of the index to element X is probed by the difference

$$\Delta\mathcal{S}_X = \mathcal{S}^f_X - \mathcal{S}^c_X \tag{59}$$

or

$$\frac{\Delta\mathcal{S}_X}{w} = \frac{\sum^w d_x}{w} - \frac{\sum^W d_x}{W} . \tag{60}$$

If $\Delta\mathcal{S}_X > 0$, then element X is proactive to the index strength (that is the index strengthens if X abundance increases) otherwise, for $\Delta\mathcal{S}_X < 0$, X is reactive (that is the index weakens if X abundance increases, as X more strongly absorbs the pseudo-continuum than the feature window). The results of our test on the Fe4531 index are displayed in the two panels of Fig. 16, for the Sun and Arcturus, respectively.

Accordingly, in Table 4 we list the five most prominent absorbers of the feature window *alone* for the Sun and Arcturus. These data definitely show that Fe is the strongest contributor to the 4531 Å blend. On the other hand, Fig. 16 also shows that Fe lines affect with a similar strength also the pseudo-continuum flux density. When netting both contributions, as in Table 5, one is left with a quite different list of prevailing chemical species that *really* settle the

Table 4. The five chemical species that are the most important contributors to the 4531 Å blend in the Sun and Arcturus spectra.

Sun		Arcturus	
Chemical species	$\mathcal{S}^a$	Chemical species	$\mathcal{S}^a$
Fe	22.3	Fe	44.0
Ti	13.5	CN	35.3
Cr	10.1	Ti	25.6
Ni	2.6	Cr	23.7
Co	2.2	Ce	11.2

Note. ^{a}According to equation (57).

Table 5. The five chemical species with the most prominent *net* sensitivity in the Fe4531 index for the Sun and Arcturus spectra.

Sun		Arcturus	
Chemical species	$\Delta\mathcal{S}^a$	Chemical species	$\Delta\mathcal{S}^a$
Ti	7.9	Ti	9.8
Cr	3.3	Cr	4.0
V	−1.4	V	−2.7
Ni	1.1	Co	1.9
Mg	−0.9	Sm	1.8
SNIa group	4.4		2.7
SNII group	−1.4		−1.0

Note. ^{a}According to equation (59).

Fe5431 behaviour. In particular, *the main driver of the index appears to be titanium (!)*, followed to a lesser extent by chromium. Note, in addition, the weak but steady inverse correlation of the index with the vanadium abundance, which acts therefore as a reactive element.

We could take our analysis further by probing the Fe4531 index response to homogeneous groups of chemical elements, like for instance the α-element chain, more directly related to SNII nucleosynthesis (Woosley & Weaver 1995), (including the combined contribution of Ca, Mg, MgH, Na, Si and SiH), or the Fe-Ni group (including Co, Cr, Fe, Mn, Ni and V), as a main by-product of SNIa activity (Nomoto et al. 1997). This is summarized in the bottom lines of Table 5. While Ti is definitely the main element that modulates Fe4531 strength, the other SNII α elements act as very weak reactive contributors, unlike the SNIa elemental group, which proactively contributes to the index strength, mainly following Cr, Co and Ni contributions. Definitely, in spite of its outstanding role, our conclusion is that Fe is quite a dull actor in this game.

4 DISCUSSION AND CONCLUSIONS

Since its definitive treatment in the early 1990s (Gorgas et al. 1993; Worthey et al. 1994), the Lick-index system has broadly become the standard in the study of stars and old stellar systems. As a successful strategy, it links the low-resolution spectroscopic approach to narrow-band photometry to deliver condensed yet essential information about all the relevant absorption features that mark the SED of an astronomical target in the 4000–6000 Å wavelength range.

Nowadays, Lick-index analysis is consistently used alongside other resources of modern extragalactic astronomy at optical wavelengths, including high-resolution spectral synthesis (e.g., Vazdekis 2001; Buzzoni et al. 2005; Rodríguez-Merino et al. 2005; Bertone et al. 2008; Vazdekis et al. 2010; Maraston & Strömbäck 2011) and low-resolution global fitting of galaxy SEDs (e.g., Massarotti, Iovino & Buzzoni 2001; Bolzonella et al. 2010; Domínguez Sánchez et al. 2011; Pforr, Maraston & Tonini 2012; González et al. 2012; Scoville et al. 2013). However, as we have discussed before, none of these is free from limitations so that narrow-band spectrophotometry still remains, in most cases, the only viable diagnostic tool to tackle with some confidence the evolutionary status of unresolved distant galaxies.

The original 21 indices of the Lick system (Worthey & Ottaviani 1997) has been complemented by including some higher-order Balmer lines (namely, Hγ and Hδ), with the aim of overcoming the possible perturbation of gas emission on the other optical features (especially Hβ) in the galaxy spectra. An alternative approach to the same problem was attempted by González (1993), to determine the Hβ emission component in the spectra of active elliptical galaxies, by using [O III] 5007 Å emission as a proxy. Although nominally not part of the original Lick system (being the only index that explicitly covers an emission feature), the [O III] index of González (1993) is often included in the extragalactic studies accompanying a more classical Lick analysis (e.g., Kuntschner et al. 2001; Prugniel, Maubon & Simien 2001; Beuing et al. 2002; Nelan et al. 2005; Ogando et al. 2008; Wegner & Grogin 2008). Overall, we can consider it as a further addition to the standard system, which amounts to a total of 26 indices (see their wavelength distribution in Fig. 1).

A recognized difficulty, when using Lick indices from different observing environments, is the standardization procedure. As we discussed in Section 2.1, this is due to the inherent difficulty with the Lick IDS set of primary stellar calibrators, originally generated by the analogical output of a video camera tube (Robinson & Wampler 1972). As a result, IDS spectra lack any stable wavelength scale and intensity response, a limitation that, by itself, constrains calibration accuracy and prevents any consistent assessment of the spectral S/N ratio (Faber & Jackson 1976; Worthey et al. 1994).

On the other hand, the problem of index standardization intimately relates to a tricky and yet not fully realized theoretical drawback. Even if both feature (*f*) and pseudo-continuum (f_c) density fluxes, as of equation (1), obey a normal distribution, the $\mathcal{R} = \overline{(f/f_c)}$ ratio may not.[4] The index definition, in terms of ratio $\mathcal{R}$, is a direct legacy of the spectroscopic mood of the Lick system, and it closely recalls the standard procedure to derive the line equivalent width as in high-resolution spectra. Given the different conditions of low-resolution unfluxed spectra, however, we have demonstrated that a somewhat alternative photometric mood should be preferred, with feature strength assessed in terms of ratio $\mathcal{R}' = (\overline{f}/\overline{f_c})$. The latter is a far more suitable and robust statistical estimator. It has a Gaussian distribution and its index strength is in terms of narrow-band colour. Under certain conditions, we have shown that $\mathcal{R}$ tends to $\mathcal{R}'$ *providing the spectrum is nearly flat and overcomes a minimum* S/N *threshold, such as*:

$$(S/N)_{\rm obs} \gtrsim 22\left(\frac{\theta}{\mathcal{W}}\right)^{1/2} \approx 5\,\theta^{1/2} \quad [{\rm px}^{-1}], \qquad (61)$$

where θ is the spectral dispersion (that is the *observed* wavelength pixel scale) and $\mathcal{W}$ the average index window size from equation (21) and Table 1. This means, for example, that for a resolving power $R \sim 2000$, a minimum $(S/N)_{\rm obs} \sim 5$ px^{-1} ratio has to be reached, assuming a Bayesian pixel fair sampling.

A relevant conclusion of our analysis is therefore that, in an effort to revise the Lick system, one should compute indices either in the classical form of the pseudo-equivalent width, relying on the classical $\mathcal{R}$ ratio of equation (1), but from previously linearized spectra according to equation (11), or (more safely) in the form of narrow-band colours of simply fluxed spectra, that is in terms of the $\mathcal{R}'$ ratio of equation (9), and express them in magnitude scale, as equation (3).

As a further issue in our analysis, in Section 3 we assessed the possible redundancy in the index information when matching for instance galaxy spectra. About 25 per cent of the covered wavelength range contributes to the definition of two or more Lick indices, a feature that may lead index changes to correlate, in some cases, beyond any strictly physical relationship. A relevant case has been explored: the nested configuration of the Fe5335, Fe5270 and Mg$_2$ indices, a classical triad often involved in literature studies to define global metallicity indices, such as the $\langle{\rm Fe}\rangle = ({\rm Fe5270} + {\rm Fe5335})/2$ of Gorgas et al. (1990), or the perused $[{\rm MgFe}] = [{\rm Mg}b\,({\rm Fe5270} + {\rm Fe5335})/2]^{1/2}$ meta-index of González (1993), in its manifold variants (see, e.g., Fritze-v. Alvensleben 1998; Thomas, Maraston & Bender 2003; Clemens et al. 2006). We have shown, in Section 3.4, that any intervening change in the Fe5335 strength is also reflected in the Mg$_2$ index (and in Mg$_1$, as well) in quite a puzzling way. One one hand, if a flux addition increases the pseudo-continuum level in common, then both Mg$_2$ and Fe5335 strengths are seen to increase, according to equation (53). On the other hand, if the Fe5335 index becomes stronger due to a deeper corresponding feature, then Mg$_2$ is seen to decrease, as equation (55).

---

[4] In some cases, the $\mathcal{R}$ ratio may even display a bi-modal statistical distribution (see Marsiglia 1964, 1965).

To embroil the situation further, in Section 3.3 we dealt with the the Mg*b* index as a tracer of the galaxy metallicity, for instance within the [MgFe] meta-index. As shown by Goudfrooij & Emsellem (1996), the strength of the Mg atomic feature itself could be tacitly modulated by the intervening gas emission, even in relatively quiescent stellar environments. The forbidden [N I] line emission about 5199 Å adds flux to the red Mg*b* pseudo-continuum (see the sketch in Fig. 10), thus leading to a stronger Mg absorption feature, overall. In Fig. 13 the effect can clearly be detected statistically by relying on the extended galaxy data base of Ogando et al. (2008). The [N I] emission is seen to correlate with the [O III] strength, roughly in the ratio 1:5, and it appears to be in excess of about 0.4 Å among the most active (i.e., [O III]-strong) objects in the sample compared with the quiescent ellipticals. According to equation (43), the Mg*b* strength is increased by a similar figure. When relying, for instance, on the empirical calibration of Pipino & Danziger (2011) to convert Lick indices into metal abundance (see, in particular, table 5, therein), *this leads to a prediction of a slightly higher metallicity, even in excess of some 0.2 dex in star-forming galaxy environments.*

Like [N I], hidden emission can subtly plague the nominal diagnostic scheme for other Lick indices. Indeed, the most debated issue in this regard deals with a fair correction of Hβ absorption in the spectra of elliptical galaxies. Compared to all the other Lick indices, Hβ (and its weaker Balmer companions, like Hγ and Hδ, see Worthey & Ottaviani 1997) is the only feature that positively correlates with the effective temperature of stars (see, e.g., fig. 4 in Trager et al. 1998). As it becomes strongest among A-type stars, this makes the index of special interest for breaking model degeneracy in the age diagnostic of old and intermediate ($t \lesssim 1$ Gyr) age galaxies (Buzzoni et al. 1994; Worthey 1994; Maraston & Thomas 2000; Tantalo & Chiosi 2004). On the other hand, as gas and stars within a galaxy conflict in their line contribution (the former, by emitting, the latter by absorbing), the integrated Hβ strength displays the net effect of this interplay.

In Section 3.2 we tackled the well-used correction procedure of González (1993), which relies on the measure of the adjacent [O III] forbidden emission at 5007 Å, as a proxy to infer the Hβ gaseous contribution. Several physical arguments question such a straightforward relationship between the two emission lines, in consequence of a range of different evolutionary mechanisms (primarily LINER activity). However, one can admittedly assume [O III] emission to be a generic (but not exclusive) tracer of star-forming activity (and the implied presence of H II gas clouds) within a young stellar population.

Taking a set of spectroscopic observations of 20 bright elliptical galaxies, originally to study radial spectrophotometric gradients (Carrasco et al. 1995; Buzzoni et al. 2009b, 2015), we devised a simple and robust diagnostic scheme to probe the possible [O III] versus Hβ entanglement. As observations were taken symmetrically across a galaxy's major axis, one can reasonably assume that whatever the distinctive evolutionary properties, the same stellar population (and, on average, gas content) is sampled at the same radial distance, on opposite sides of the galaxy centre. If this is the case, then the Hβ and [O III]$_{5007}$ index differences between the two galaxy sides can be contrasted in a search for possible statistical correlations. One major advantage of this approach is that it is nominally free from zero-point and other calibration problems with the data, just relying on the assumed central symmetry of the galaxy stellar population.

Our results, summarized in Fig. 8 and Table 3, basically confirm the correction figure of $\Delta H\beta/\Delta[\mathrm{O\,III}]_{5007} \sim 0.7 \pm 0.5$ (González 1993), but only for those ellipticals with established ongoing star-formation activity and stronger core emission (i.e., $[\mathrm{O\,III}]_{5007} \lesssim -1.5$ Å). For more quiescent galaxies, any Hβ emission is found to fade out more quickly than [O III]$_{5007}$ emission, and this suggests a milder correction scheme, which we parametrized with a logistic curve (see Fig. 9), as in equations (33) and (34).

The effect of our Hβ correction can be appreciated by looking again at the Ogando et al. (2008) sample of elliptical galaxies (Fig. 17). The corrected galaxy distribution in the Hβ versus Mg$_2$ plane is shown in the right-hand panel of the figure, compared with the original sample in the left-hand panel. As a guideline, the Buzzoni et al. (1994) models are overplotted, throughout. Notice that most of the galaxies with shallow (or negative) Hβ in the left-hand panel are effectively recovered by the procedure, leading eventually to a much cleaner Hβ versus Mg$_2$ relationship. Along the whole galaxy sample, the corrected Hβ index slightly increases, on average, by $\Delta \mathrm{H}\beta \simeq 0.25 \pm 0.20$ Å. Although apparently negligible, this figure has important impacts on the inferred galaxy age, which typically shifts towards 20–30 per cent younger values with a 0.2–0.3 dex poorer inferred metallicity (Buzzoni et al. 1994; Worthey 1994).

Apart from the Hβ problem, the striking importance of the [O III]$_{5007}$ forbidden line also emerged in our discussion in Section 3.2 when dealing with the intrinsic strength of the Fe5015 index. On one hand, any intervening [O III]$_{5007}$ emission will decrease Fe5015 strength as it adds flux to the feature window of the latter. On the other hand, the broader and stronger Fe5015 absorption in the integrated spectrum of old stellar populations may artificially depress the apparent [O III]$_{5007}$ luminosity, thus leading to an underestimate of its equivalent width. In our analysis, we tackled in some detail the problem of a mutual correction of the two indices, devising a general procedure that could straightforwardly be applied to other similar contexts. The intrinsic [O III]$_{5007}$ strength can therefore be derived in terms of observed quantities, via equation (31), while the intrinsic Fe5015 index, corrected for O emission, is simply derived from equation (27).

One important consequence of our analysis is that the corrected Fe5015 index is generally expected to increase in the galaxy spectrum, opposite to the Mg*b* trend. This feature may have some impact when combining the two indices, like in the [MgFe50] meta-index, so extensively used, for instance, in the SAURON studies (Kuntschner et al. 2010; Falcón-Barroso et al. 2011). An interesting comparison can be done, in this regard, with Peletier et al. (2007, see, in particular, their fig. 3). In the plot, when taking the stellar population synthesis models of Thomas et al. (2003) as a reference in the Fe5015 versus Mg*b* domain, it appears that SAURON ellipticals better match the α-enhanced models with respect to the standard solar chemical partition. On the other hand, one may argue that this is the natural consequence of a relatively strong Mg*b* and shallow Fe5015, so that, when accounting for the envisaged corrections, the net effect on the fit is to mitigate any inferred α-element enhancement of the galaxy population.

Because of its relevance, the Mg index complex (including Mg*b*, Mg$_1$ and Mg$_2$ indices) was the focus of our specific analysis in Section 3.3. In its original intention, the Lick system aimed at singling out the atomic and molecular contribution to the broad Mg valley about 5150 Å (Faber et al. 1977). This evidently leads to some entanglement among the three indices, which we theoretically assessed for the first time with equation (38). This inherent relationship can be usefully relied upon for incomplete spectral observations, either to derive the missing index (within a ∼1.5 per cent internal accuracy) given the other two or, even more importantly,

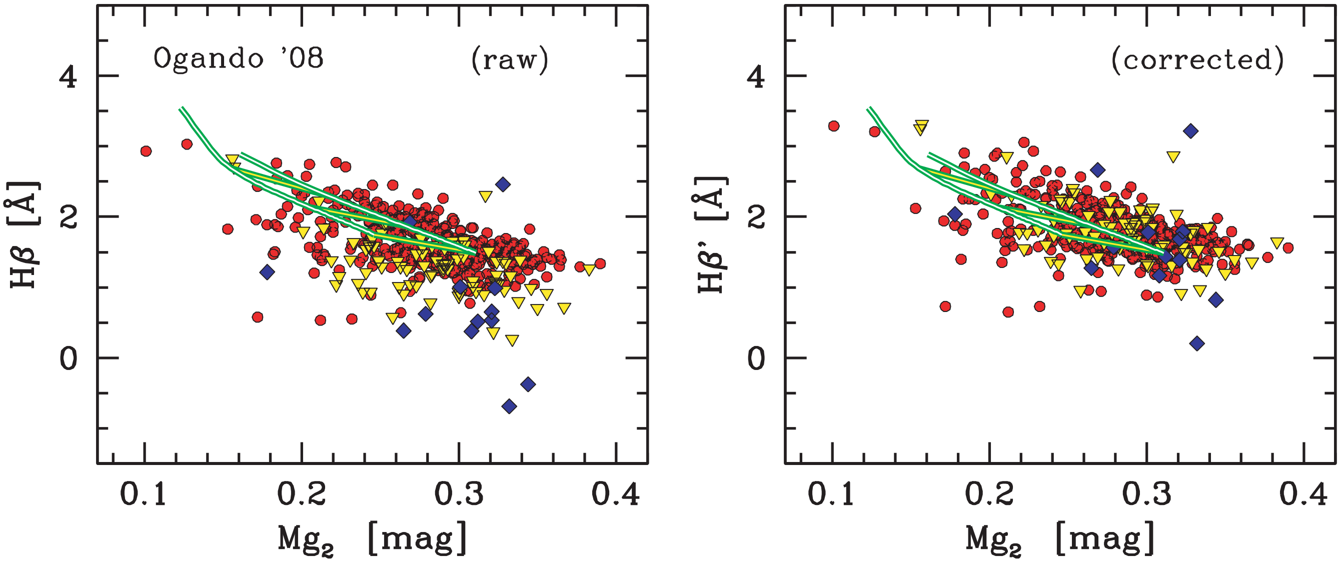

Figure 17. Devised scheme for Hβ correction, as in Fig. 9, applied to the early-type galaxy sample of Ogando et al. (2008), displayed in the Hβ versus Mg$_2$ index plane. The strength of Hβ_e gas emission is determined and subtracted according to equation (34), taking the observed $[\mathrm{O\,III}]'_{5007}$ emission as a proxy. To appreciate the correction effect better, we adopted three different galaxy markers for nearly quiescent (i.e., $[\mathrm{O\,III}]'_{5007} > -1$ Å or H$\beta_e \gtrsim -0.4$ Å, solid dots), moderately active ($-2 \le [\mathrm{O\,III}]'_{5007} \le -1$ Å or $-1.5 \lesssim$ H$\beta_e \lesssim -0.4$ Å, triangles) and active (i.e., $[\mathrm{O\,III}]'_{5007} < -2$ Å or H$\beta_e \lesssim -1.5$ Å, rhombi) galaxies. As a guideline, in both panels we also display the synthesis models of Buzzoni et al. (1994) for a standard Salpeter initial mass function and [Fe/H] metallicity parameter between -0.25 (upper line) and $+0.22$ dex (lower line). The ladders across the model sequences tick galaxy age for values of 2, 5, 10 and 15 Gyr, with increasing Mg$_2$. After correction (right-hand panel), galaxy Hβ index is increased, on average, by 0.25 ± 0.20 Å along the whole sample, making galaxies appear, on average, about 20–30 per cent younger and 0.2–0.3 dex metal poorer.

to assess any possible deviation from the standard scheme due to intervening bias effects in the spectra. This has actually been our approach, for instance, to single out the $[\mathrm{N\,I}]_{5199}$ contribution, as shown in Fig. 13.

For low-resolution spectra, as in any Lick analysis, we are left with the inescapable consequence that any absorption feature is a blend of a coarse elemental contribution. As we have shown in Section 3.5, this problem has been widely explored, from a theoretical point of view, in the recent literature (the work of Serven et al. 2005 is probably the most up-to-date attempt in this sense), which assesses index responsiveness to the different chemical species that may potentially intervene at the relevant wavelength of the blended absorption feature. On the other hand, notice that, because of its inherent definition, the strength of the Lick index directly stems from the *residual* in-band elemental contribution to the feature itself, compensated by the corresponding off-band contribution to the flanking pseudo-continuum. Unlike high-resolution spectroscopy, therefore, a tricky situation may actually occur, where the Lick-index christening element (the one with the deepest absorption within the feature window) is not necessarily the representative one that constrains the index strength, as a whole.

As a recognized example (Trager et al. 1998; Serven et al. 2005), in Section 3.5 we reconsidered in somewhat finer detail Fe4531, one among the many *bona fide* iron tracers in the optical spectrum of galaxies, according to the classical Lick scheme. For our analysis, we relied on observed spectra of the Sun and Arcturus as typical main-sequence and red-giant stellar templates, in an attempt to extend our conclusions also to the old-galaxy framework, according to more elaborated stellar population synthesis models. A comparison of Tables 4 and 5 is illuminating for catching the sense of our analysis.

In Table 4, both for the Sun and Arcturus (and, by inference, in the spectrum of elliptical galaxies, for instance), *iron* is undoubtedly the leading contributor to the absorption feature at 4531 Å, but once the Fe coarse absorption in the nearby pseudo-continuum has been cleared, it is actually *titanium* that, almost solely, commands the game (Table 5) and eventually modulates Fe4531 index behaviour. As a final consideration, Fe4531 and more generally the essence of all our previous discussion, evidently urge an important rethinking of the Lick-index tool, to bring it fresh life and to tune it even better for diagnostic performance in view of its updated application to the new-generation spectral data to come.

ACKNOWLEDGEMENTS

The anonymous referee is warmly acknowledged for his/her competent and very careful review of the draft, and for a number of timely suggestions, all of which had special relevance for focusing our analysis better. This work has made extensive use of the SPECTROWEB 1.0 interactive data base of spectral standard star atlases, maintained by Alex Lobel and collaborators at the Royal Observatory of Belgium in Brussels.

REFERENCES

Bernardi M., Nichol R. C., Sheth R. K., Miller C. J., Brinkmann J., 2006, AJ, 131, 1288
Bertone E., Buzzoni A., Rodríguez-Merino L. H., Chávez M., 2004, Mem. Soc. Astron. Ital., 75, 158
Bertone E., Buzzoni A., Chávez M., Rodríguez-Merino L. H., 2008, A&A, 485, 823
Bettoni D., Buson L. M., 1987, A&AS, 67, 341
Beuing J., Bender R., Mendes de Oliveira C., Thomas D., Maraston C., 2002, A&A, 395, 431
Bolzonella M. et al., 2010, A&A, 524, AA76
Bressan A., Chiosi C., Tantalo R., 1996, A&A, 311, 425
Brodie J. P., Huchra J. P., 1990, ApJ, 362, 503

Burstein D., Faber S. M., Gaskell C. M., Krumm N., 1984, ApJ, 287, 586
Buzzoni A., 1995, ApJS, 98, 69
Buzzoni A., Gariboldi G., Mantegazza L., 1992, AJ, 103, 1814
Buzzoni A., Mantegazza L., Gariboldi G., 1994, AJ, 107, 513
Buzzoni A., Chavez M., Malagnini M. L., Morossi C., 2001, PASP, 113, 1365
Buzzoni A., Bertone E., Rodríguez-Merino L. H., Chávez M., 2005, in Renzini A., Bender R., eds, Proc. ESO Workshop, Multiwavelength Mapping of Galaxy Formation and Evolution. ESO, Garching, p. 361
Buzzoni A., Bertone E., Chavez M., 2009a, ApJ, 703, L127
Buzzoni A., Battistini C., Carrasco L., Recillas E., 2009b, Rev. Mex. Astron. Astrofis. Conf. Ser., 37, 110
Buzzoni A., Salsa M., Battistini C., Carrasco L., Recillas E., 2015, ApJ, in preparation
Caldwell N., 1984, PASP, 96, 287
Cappellari M. et al., 2011, MNRAS, 413, 813
Cardiel N., Gorgas J., Cenarro J., Gonzalez J. J., 1998, A&AS, 127, 597
Carollo C. M., Danziger I. J., Buson L., 1993, MNRAS, 265, 553
Carrasco L., Buzzoni A., Salsa M., Recillas-Cruz E., 1995, in Buzzoni A., Renzini A., Serrano A., eds, ASP Conf. Ser. Vol. 86, Fresh views of elliptical galaxies., Astron. Soc. Pac., San Francisco, p. 235
Carson D. P., Nichol R. C., 2010, MNRAS, 408, 213
Clemens M. S., Bressan A., Nikolic B., Alexander P., Annibali F., Rampazzo R., 2006, MNRAS, 370, 702
Coelho P., Barbuy B., Meléndez J., Schiavon R. P., Castilho B. V., 2005, A&A, 443, 735
Colless M., Burstein D., Davies R. L., McMahan R. K., Saglia R. P., Wegner G., 1999, MNRAS, 303, 813
Conroy C., 2013, ARA&A, 51, 393
Crocker A. F., Bureau M., Young L. M., Combes F., 2011, MNRAS, 410, 1197
Davies R. L., Burstein D., Dressler A., Faber S. M., Lynden-Bell D., Terlevich R. J., Wegner G., 1987, ApJS, 64, 581
de Vaucouleurs G., de Vaucouleurs A., Corwin H. G., Jr, Buta R. J., Paturel G., Fouque P., 1991, Third Reference Catalog of Bright Galaxies. Springer Verlag, Heidelberg
Dobos L., Csabai I., Yip C.-W., Budavári T., Wild V., Szalay A. S., 2012, MNRAS, 420, 1217
Domínguez Sánchez H. et al., 2011, MNRAS, 417, 900
Faber S. M., 1973, A&AS, 10, 201
Faber S. M., Jackson R. E., 1976, ApJ, 204, 668
Faber S. M., Burstein D., Dressler A., 1977, AJ, 82, 941
Faber S. M., Friel E. D., Burstein D., Gaskell C. M., 1985, ApJS, 57, 711
Falcón-Barroso J. et al., 2011, MNRAS, 417, 1787
Ferland G. J., Henney W. J., O'Dell C. R., Porter R. L., van Hoof P. A. M., Williams R. J. R., 2012, ApJ, 757, 79
Fritze-v. Alvensleben U., 1998, in Andersen J., ed., Highlights of Astronomy, Vol. 11, Kluwer Academic Publishers, Dordrecht, p. 78
Fusi Pecci F., Bellazzini M., Buzzoni A., De Simone E., Federici L., Galleti S., 2005, AJ, 130, 554
Geary R. C., 1930, J. R. Statistical Soc., 93, 442
Golay M., 1974, Introduction to Astronomical Photometry, Astrophysics & Space Science Library, Vol. 41, Reidel, Dordrecht
González J. J., 1993, PhD thesis, Univ. Santa Cruz
González V., Bouwens R. J., Labbé I., Illingworth G., Oesch P., Franx M., Magee D., 2012, ApJ, 755, 148
Gorgas J., Efstathiou G., Aragon Salamanca A., 1990, MNRAS, 245, 217
Gorgas J., Faber S. M., Burstein D., Gonzalez J. J., Courteau S., Prosser C., 1993, ApJS, 86, 153
Goudfrooij P., Emsellem E., 1996, A&A, 306, L45
Hayya J., Armstrong D., Gressis N., 1975, Management Sci., 21, 1338
Hinkley D. V., 1969, Biometrika, 56, 635
Huber K. P., Herzberg G., 1979, in Linstrom P. J., Mallard W. G., eds, Constants of Diatomic Molecules (data prepared by Gallagher J. W., Johnson R. D. III), NIST Chemistry WebBook, NIST Standard Reference Database Number 69, American Elsevier, New York
Kaler J. B., 1980, ApJ, 239, 592
Kehrig C. et al., 2012, A&A, 540, AA11
Kennicutt R. C., Jr, 1992, ApJ, 388, 310
Kewley L. J., Dopita M. A., 2002, ApJS, 142, 35
Kobayashi C., Arimoto N., 1999, ApJ, 527, 573
Kuntschner H., Lucey J. R., Smith R. J., Hudson M. J., Davies R. L., 2001, MNRAS, 323, 615
Kuntschner H. et al., 2006, MNRAS, 369, 497
Kuntschner H. et al., 2010, MNRAS, 408, 97
Kupka F., Piskunov N., Ryabchikova T. A., Stempels H. C., Weiss W. W., 1999, A&AS, 138, 119
Lobel A., 2007, in Gomez de Castro A., Barstow M., eds, Proc. Ultraviolet Universe: Stars from Birth to Death, 26th Meeting of the IAU. Complutense Univ., Madrid, p. 167
Lobel A., 2008, Proc. 9th Int. Colloq. Atomic Spectra and Oscillator Strengths for Astrophysical and Laboratory Plasmas, J. Phys. Conf. Series, 130, 012015
Lobel A., 2011, Canadian J. Phys., 89, 395
Maraston C., Strömbäck G., 2011, MNRAS, 418, 2785
Maraston C., Thomas D., 2000, ApJ, 541, 126
Marsiglia G., 1964, Mathematical Notes. Boeing Scientific Research Lab., p. 138
Marsiglia G., 1965, J. American Statistical Association, 60, 193
Massarotti M., Iovino A., Buzzoni A., 2001, A&A, 368, 74
McClure R. D., van den Bergh S., 1968, AJ, 73, 313
Mollá M., Hardy E., Beauchamp D., 1999, ApJ, 513, 695
Mould J. R., 1978, ApJ, 220, 434
Moustakas J., Kennicutt R. C., Jr, Tremonti C. A., 2006, ApJ, 642, 775
Nelan J. E., Smith R. J., Hudson M. J., Wegner G. A., Lucey J. R., Moore S. A. W., Quinney S. J., Suntzeff N. B., 2005, ApJ, 632, 137
Nomoto K., Iwamoto K., Nakasato N., Thielemann F.-K., Brachwitz F., Tsujimoto T., Kubo Y., Kishimoto N., 1997, Nucl. Phys. A, 621, 467
Ogando R. L. C., Maia M. A. G., Pellegrini P. S., da Costa L. N., 2008, AJ, 135, 2424
Öhman Y., 1934, ApJ, 80, 171
Osterbrock D. E., 1974, Astrophysics of Gaseous Nebulae and Active Galactic Nuclei. Univ. Sci. Books, Mill Valley
Pagel B. E. J., 1997, Nucleosynthesis and Chemical Evolution of Galaxies. Cambridge Univ. Press, Cambridge
Pagel B. E. J., Edmunds M. G., Blackwell D. E., Chun M. S., Smith G., 1979, MNRAS, 189, 95
Papaderos P. et al., 2013, A&A, 555, LL1
Peletier R. F. et al., 2007, MNRAS, 379, 445
Pérez I., Sánchez-Blázquez P., Zurita A., 2009, A&A, 495, 775
Pforr J., Maraston C., Tonini C., 2012, MNRAS, 422, 3285
Phillips M. M., Jenkins C. R., Dopita M. A., Sadler E. M., Binette L., 1986, AJ, 91, 1062
Pipino A., Danziger I. J., 2011, A&A, 530, A22
Piskunov N. E., Kupka F., Ryabchikova T. A., Weiss W. W., Jeffery C. S., 1995, A&AS, 112, 525
Prugniel P., Maubon G., Simien F., 2001, A&A, 366, 68
Rich R. M., 1988, AJ, 95, 828
Robinson L. B., Wampler E. J., 1972, PASP, 84, 161
Rodríguez-Merino L. H., Chavez M., Bertone E., Buzzoni A., 2005, ApJ, 626, 411
Rogers B., Ferreras I., Peletier R., Silk J., 2010, MNRAS, 402, 447
Sachs L., 1984, Applied Statistics. Springer Verlag, New York
Sánchez-Blázquez P., Gorgas J., Cardiel N., González J. J., 2006a, A&A, 457, 787
Sánchez-Blázquez P., Gorgas J., Cardiel N., González J. J., 2006b, A&A, 457, 809
Sandage A., 1969, ApJ, 158, 1115
Sarzi M. et al., 2006, MNRAS, 366, 1151
Sarzi M. et al., 2010, MNRAS, 402, 2187
Scoville N. et al., 2013, ApJS, 206, 3
Serven J., Worthey G., Briley M. M., 2005, ApJ, 627, 754
Smith P. L., Esmond J. R., Heise C., Kurucz R. L., 1996, in Yamashita K., Watanabe T., eds, On-Line Atomic and Molecular Data for Astronomy, in UV and X-ray Spectroscopy of Astrophysical and Laboratory Plasmas. Universal Academy Press, Tokyo, p. 513

Spinrad H., Taylor B. J., 1969, ApJ, 157, 1279

Spinrad H., Wood D. B., 1965, ApJ, 141, 109

Strömgren B., 1956, Vistas Astron., 2, 1336

Tantalo R., Chiosi C., 2004, MNRAS, 353, 917

Tantalo R., Chiosi C., Bressan A., 1998, A&A, 333, 419

Thomas D., Maraston C., Bender R., 2003, MNRAS, 339, 897

Thomas D., Maraston C., Bender R., Mendes de Oliveira C., 2005, ApJ, 621, 673

Trager S. C., Worthey G., Faber S. M., Burstein D., Gonzalez J. J., 1998, ApJS, 116, 1

Trager S. C., Faber S. M., Worthey G., González J. J., 2000, AJ, 119, 1645

Tripicco M. J., Bell R. A., 1995, AJ, 110, 3035

Vazdekis A., 2001, Ap&SS, 276, 921

Vazdekis A., Casuso E., Peletier R. F., Beckman J. E., 1996, ApJS, 106, 307

Vazdekis A., Sánchez-Blázquez P., Falcón-Barroso J., Cenarro A. J., Beasley M. A., Cardiel N., Gorgas J., Peletier R. F., 2010, MNRAS, 404, 1639

Volkov E. V., 1990, Astrophysics, 32, 80

Vollmann K., Eversberg T., 2006, Astron. Nachr., 327, 862

Walcher C. J., Böker T., Charlot S., Ho L. C., Rix H.-W., Rossa J., Shields J. C., van der Marel R. P., 2006, ApJ, 649, 692

Walcher J., Groves B., Budavári T., Dale D., 2011, Ap&SS, 331, 1

Wegner G., Grogin N. A., 2008, AJ, 136, 1

Wood D. B., 1963, PhD thesis, Univ. California, Berkeley

Woosley S. E., Weaver T. A., 1995, ApJS, 101, 181

Worthey G., 1994, ApJS, 95, 107

Worthey G., 1996, in Leitherer C., Fritze-von Alvensleben U., Huchra J., eds, Astronomy Society of the Pacific Conference Series Vol. 98, From Stars to Galaxies. Astron. Soc. Pac., San Francisco, p. 467

Worthey G., Ottaviani D. L., 1997, ApJS, 111, 377

Worthey G., Faber S. M., Gonzalez J. J., Burstein D., 1994, ApJS, 94, 687

This paper has been typeset from a TEX/LATEX file prepared by the author.